IEEE Access
Multidisciplinary ⋮ Rapid Review ⋮ Open Access Journal

Received 10 October 2023, accepted 30 October 2023, date of publication 8 November 2023, date of current version 27 November 2023.

*Digital Object Identifier 10.1109/ACCESS.2023.3331567*

RESEARCH ARTICLE

# Peer-to-Peer-Based Power Flow Control in Microgrids With Limited Voltage Harmonic Distortion

**STEVAN GRABIĆ, (Member, IEEE), MARKO VEKIĆ, (Member, IEEE), MILAN RAPAIĆ, (Member, IEEE), IVANA ISAKOV, AND VLADO POROBIĆ, (Member, IEEE)**
Faculty of Technical Sciences, University of Novi Sad, 21000 Novi Sad, Serbia

Corresponding author: Marko Vekić (vekmar@uns.ac.rs)

This work was supported by the Ministry of Science, Technological Development and Innovation through the "Innovative Scientific and Artistic Research From the Faculty of Technical Sciences Activity Domain" under Project 451-03-47/2023-01/200156.

**ABSTRACT** This paper proposes a novel primary level controller and coupling LCL filter design methodology for microgrid prosumer units The so-called decentralized peer-to-peer-based power flow control algorithm introduces a power exchange communication link between two contractees, namely a prosumer unit and any other unit, on the time scales of primary power flow controller. This can be regarded as feed-forwarding of power flow information between the units in close to real-time in order to attain almost instant power balancing within the system. When coupled with the conventional voltage and frequency droop primary control, as presented in the paper, and tested on a simulation model of one radial microgrid in the off-grid mode of operation, it showed enhanced static and dynamic performance. The study also investigated adverse influence of the communication link time delay. The paper addressed prosumer units microgrid voltage-forming role by proposing design and control methodology for the prosumer units' LCL coupling filter. To that aim, thorough voltage and current harmonic emission analysis has been conducted, taking into account realistic span of a microgrid parameters' values and presence of other units. The study and the simulation model tests revealed that the limited total voltage harmonic distortion becomes critical requirement in the off-grid model of operation.

**INDEX TERMS** Microgrid, peer-to-peer power flow, decentralized control, droop control, limited voltage and current THD, LCL filter design, active damping.

## LIST OF ACRONYMS

| | |
|---|---|
| PU | Prosumer Unit. |
| V2G | Vehicle-to-Grid. |
| MG | Microgrid. |
| DSO | Distribution System Operator. |
| P2P | Peer-to-Peer. |
| PCC | Point-of-Common-Coupling. |
| DT | Distribution Transformer. |
| EV | Electric Vehicle. |
| PLL | Phase-Locked-Loop. |
| HD | Harmonic Distortion. |
| THD | Total Harmonic Distortion. |
| DG | Distributed Generator. |
| IoT | Internet-of-Things. |

The associate editor coordinating the review of this manuscript and approving it for publication was Salvatore Favuzza.

## I. INTRODUCTION

Recent developments in electric power grids have been strongly governed by the introduction of large-scale renewable power sources and distributed generation units. This technological drift [1] has yielded a drift in investment policy where the private initiative has taken the driving seat from public companies and governments [2]. Now, it is foreseen that the trend will spread to the level of individual consumers that would undertake further introduction of renewables and installation of new grid management capacities [3], such

as demand-side response, energy storage units, DC energy distribution, electric vehicle to grid (V2G) services, etc.

In this process, consumers will be transformed into so-called ''prosumers'' (producers/consumers). On the power hardware side, the prosumer unit (PU), shown in the Fig. 1, interfaces local loads, energy sources, and storage with the microgrid (MG) or the power grid. The energy storage, usually coupled to the PU's DC bus, is indispensable in this concept.

Naturally, the prosumer expects some privileges for the investment [2]. To make the grounds for such a scenario, regulatory bodies, commissions, and governments have brought directives for the decentralization and liberalization of grid infrastructure [4]. To date, two distinct grid decentralization concepts have been scientifically addressed and field-tested on the pilot systems: distributed peer-to-peer (P2P) power exchange [5], [6] and the microgrid (MG) concept [7], [8].

The P2P energy exchange deals with the broad scope of liberalized distribution grid operation aspects, including topology [9], management [10], process monitoring [11], and economics. P2P is primarily concerned with on-grid operation with a central unit (agent) that manages energy exchange between prosumers. A detailed study how prosumers may track power references coming from P2P contracts together with hierarchical control in autonomous microgrids or nanogrids is offered in [12]. Here, the time scales involved in managing active and reactive power flows are in the range of minutes [6].

On the other hand, the MG concept is mainly focused on the islanded mode of operation, where voltage and frequency stability are of primary concern. There are three main approaches in MG management and control that directly affect the operation of each prosumer: a) master-slave approach [13], b) distributed control [14], and c) decentralized control [8], [15]. Although the MG is supposed to be an autonomous entity of the distribution grid, its internal organization tends to be centralistic. The reason for that is the main objective – to divide the total MG loading among PUs so that their relative power outputs are the same [15].

P2P and MG setups correlate differently with potential for a seamless transition from the current grid concept and stability. The P2P approach is much more in favor of seamless transition, as prosumers, the grid, and the DSO would need to adopt a certain communication infrastructure and interlink over the few data acquisition and processing centers [11]. On the other hand, the MG concept requires much more than a fit to the system. It relies on the grid-tie converter at each prosumers' site and demanding communication [16], [17], data acquisition, and data processing layers [18].

Regarding stability, the MG provides superior characteristics. MG voltage and frequency are controlled in the presence of varying energy production and consumption, disturbances [19], and faults [20]. Also, thanks to the responsiveness of the grid-tie power electronic converter, MG concept can provide some extra benefits, like active compensation of nonlinear

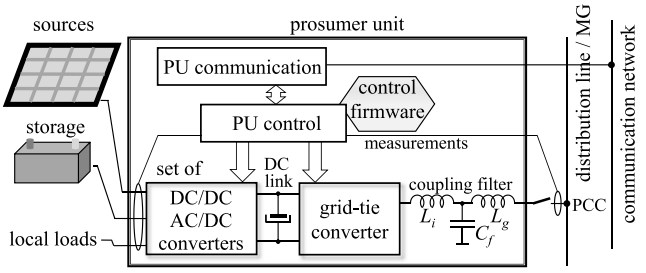


**FIGURE 1.** Prosumer unit setup.

loads current harmonics [21], [22], [23] or unified power quality conditioning [24]. In [25] the algorithm that minimizes the voltage THD while ensuring a degree of current harmonic sharing between distributed generators was proposed. The role of the grid-tie converter can be made further versatile, e.g. by operating it as series active filter to compensate voltage harmonics and enhance MG stability [26]. Such system disturbances, operation fault and power quality modes are beyond the P2P control bandwidth. Generally, P2P systems, implemented on both smaller and wider scales, rely on the grid's stiffness and stability.

Motivated by the advantages and disadvantages of the P2P and MG solutions, and intrigued by the rough technological partition between them, this paper proposes a novel - decentralized P2P-based power flow control MG concept. It belongs to the class of decentralized MG concepts, which incorporates almost real-time P2P power exchange between any of the units. The real-time P2P power transfer is attained by coupling energy trading, the communication layer, and the PU's controllable energy conversion. The role of the communication layer is to direct power flow from the sourcing point to the syncing point. For example, if two parties have agreed to exchange a certain amount of power at a given period of time, the sourcing party would increase its power production while the sinking party would simultaneously start consuming the same amount of power. With such capacity to provide dynamic energy balance in the MG system, trading and communication layers are becoming a major stabilization medium.

The second goal of the paper is to introduce design procedure for the LCL coupling filter and its control that would provide the required energy interface between the PU and the MG in the on-grid and off-grid modes of operation. Namely, existing LCL filter design methodologies and testing procedures cover solely the converter's on-grid mode of operation [27], [28], [29]. However, in the off-grid mode, the MG connection requirements are not established, and many details, regarding converter interaction with the MG environment are still missing. The paper proposes solution based on the current and voltage harmonic distortion analysis of the system, which covers edge-cases regarding the number of PUs, different types of loads and MG parameters in the span of expected values. The analysis has shown that LCL filter design procedure has to be complemented with the

requirement to attain limited total voltage harmonic distortion as the critical criterion in the off-grid mode of operation.

## II. DECENTRALIZED P2P BASED POWER FLOW PRIMARY CONTROL

The microgrid containing PUs, has been anticipated in this paper with the presumption of the seamless transition from the classical distribution network [7]. As shown in Fig. 2, the MG is a part of the classical distribution network. It consists of one or several radial distribution lines, i.e. feeders streaming from the same distribution transformer's (DT's) busbar, which has a common circuit breaker enabling the MG's connection and disconnection from the rest of the distribution grid and the distribution transformer. The number of feeders, the MG's voltage level and its structure depend on the type of network (city or rural), the number and type of consumers (residential, commercial, or industrial), and their spatial distribution. It is also assumed that the MG would retain the radial structure in both the on-grid and off-grid modes of operation, being the state in the vast majority of cases.

The control methodology of the PU should bear the same presumption of seamless transition and scalability. The seamless transition requires that PU should host uncontrollable loads, intermittent renewable energy sources, different storage units, EV chargers, and others. The PU should support the stability of the MG's service. From the scalability point of view, the introduction of a new PU should not require a significant increase in the management effort (measured in the computation and/or communication load) from any existing grid unit or other elements of the infrastructure.

A possible solution to this problem is the introduction of peer-to-peer (P2P) energy exchange on the MG level and its coupling with the primary (power flow) control task utilizing the communication layer. In this paper, the concept is referred to as ''decentralized P2P based power flow control''.

There are three possible power-exchanging options between different units that can communicate their power throughput. In the first case, the contractees are two PUs. The power is routed from one PU to another. Here, one of them is communicating the power reference values and corresponding timestamps (time identifiers of the power references' changes).

In the second case, the power is routed from the PU to an uncontrollable load that has instantaneous power consumption measurement with access to the communication link. Here the communicated power consumption becomes power reference for the PU. The timestamping is not possible in this case. The third case is similar to the second case, with the opposite power flow: an intermittent power source feeds power to the PU. In order for the second and third case to be materialized, it is required that the communication should be carried out in sufficiently small time samples and small latency so that the PU's power intake follows in close-to-real-time intermittent source's power output. This way the P2P power-exchange communication can accomplish

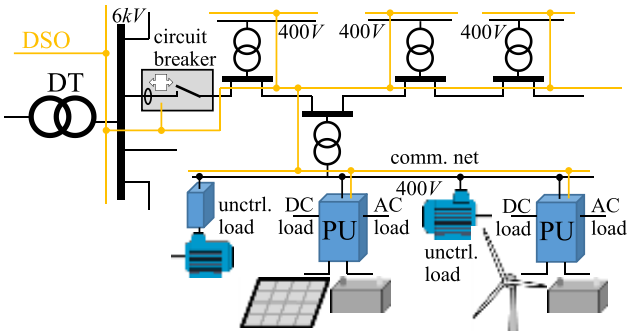


**FIGURE 2.** An example of the microgrid layout.

the feed-forwarding effect to the power flow control. Such approach has a huge positive consequence by means that the perturbations in the generation and consumption are no more interruptions to the system but have become control variables.

The PU's primary control study presented in this paper is focused on the MG islanded mode of operation. To make the control objective relatively easy to perceive, the MG power lines were considered predominantly inductive, $X_m > R_m$ ($X_m$ – line reactance, $R_m$ – line resistance). This leads to a relatively clear dependency between the established power flows and grid variables, where the active power flow mainly affects the grid frequency, whereas the reactive power flow principally influences the grid voltage [18].

There are two control actions for the primary controller to carry out simultaneously: 1) to execute bilateral agreement(s) with the other PUs and uncontrollable loads in the close-to-real-time and 2) to participate in the MG system voltage and frequency regulation to their prescribed levels. The fact that the fulfillment of the first task may make the grid variables go out of the bounds in a steady-state and in transitional periods, for example, because of the voltage drop on the line impedances, the communication time delays, etc., indicate that the two actions are intrinsically coupled and should act cooperatively. In addition, there may exist some other sources of MG disturbances, such as controllable or uncontrollable units that do not participate in P2P power flow control, units that do not fulfill their contracts at a particular time (referred to as the disrupting units), etc. PUs need to tackle these disturbances in a controllable manner.

The solution suggested in this paper is an extension of the conventional droop control technique [15]. It includes the control of the PU's output angular frequency, $\omega$, with respect to its instantaneous active power output, $p$, in the form

$$\omega = \omega_N + K_\omega \cdot \left( p - \frac{P_N}{2} - p_{PP} \right) + d\omega, \tag{1}$$

and the control of the PCC voltage magnitude $U$ with respect to its instantaneous reactive power output, $q$:

$$U = U_N + K_u \cdot (q - q_{PP}) + dU. \tag{2}$$

The extension includes two new terms in (1) and (2): peer-to-peer contracted instantaneous active power ($p_{PP}$) and

peer-to-peer contracted instantaneous reactive power ($q_{PP}$). The other parameters in (1) and (2) are: $\omega_N$ is the nominal grid frequency (e.g., $\omega_N = 314$ rad/s), $P_N$ is the PU's rated active power, $K_\omega$ is the $p$-$\omega$ droop control gain, $d\omega$ is the corrective frequency term issued by the secondary controller, $U_N$ is the nominal grid voltage (here $U_N = 3{,}3$ kV), $K_u$ is the $q$-$u$ droop control gain, and $dU$ is the corrective voltage term issued by the secondary controller. The principal advantage of such extensions is that they foster peer-to-peer power flows exclusively between the contractees. Since the information about required amount of active and reactive power is feed-forwarded between a consumer and a producer, the process of power exchange should have significantly smaller impact on the system's stability as tests in Chapter V will demonstrate.

In the form of the control characteristics, expressions (1) and (2) are shown in Fig. 3.a and Fig. 3.b, respectively. The control parameter $K_\omega$ determines the slope of the $p$–$\omega$ characteristic and $K_u$ determines the slope of the $q$-$u$ characteristic, which are set as follows:

$$K_\omega = -\frac{\Delta\omega_N}{P_N}; \quad K_u = -\frac{\Delta U_N}{Q_N} \tag{3}$$

where $\Delta\omega_N$ is the nominal angular frequency deviation range (e.g., 2%· of 314 rad/s) and $\Delta U_N$ is the nominal grid voltage deviation range (e.g., 20%· of 3.3 kV).

The implementation of the given control law within the PU's primary controller includes the following steps (see Fig. 4.a and 4.b):

- calculation of the PU's output voltage phase angle $\theta$:

$$\theta = \int_0^t \omega \cdot dt + \theta_{PLL(t=0)}, \tag{4}$$

where $\theta_{PLL(t=0)}$ is the phase angle of the PCC voltage detected by the phase-locked loop (PLL) block at the moment of the PU synchronization to the MG ($t = 0$)

- calculation of the primary controller output voltage magnitude, $U_P$:

$$U_P = K_{Pu} \cdot e_u + K_{Iu} \cdot \int_0^t e_u \cdot d\tau + U_{PLL(t=0)},$$
$$e_u = U - U_{PLL} \tag{5}$$

where $K_{Pu}$ is the proportional gain, $K_{Iu}$ is the integral gain of the PI controller that adjust the $U_P$ to compensate for the voltage drop on the LCL coupling filter; $e_u$ is the difference between the reference value of the PCC voltage magnitude, $U$, and the magnitude of the PCC voltage detected by the PLL, $U_{PLL}$; $U_{PLL(t=0)}$ is the value of $U_{PLL}$ at the moment of synchronization.

- the transformation of the three-phase voltage signal $U_P\angle\theta$ into $dq$ synchronous reference frame oriented signals $u_{Pd}$ and $u_{Pq}$, based on the angle $\theta_{PLL}$. The obtained signals are finally added to the coupling filter active damping components $u_{Ad}$ and $u_{Aq}$ to form the output voltage of the PU, $u_i$ (see Fig. 7).

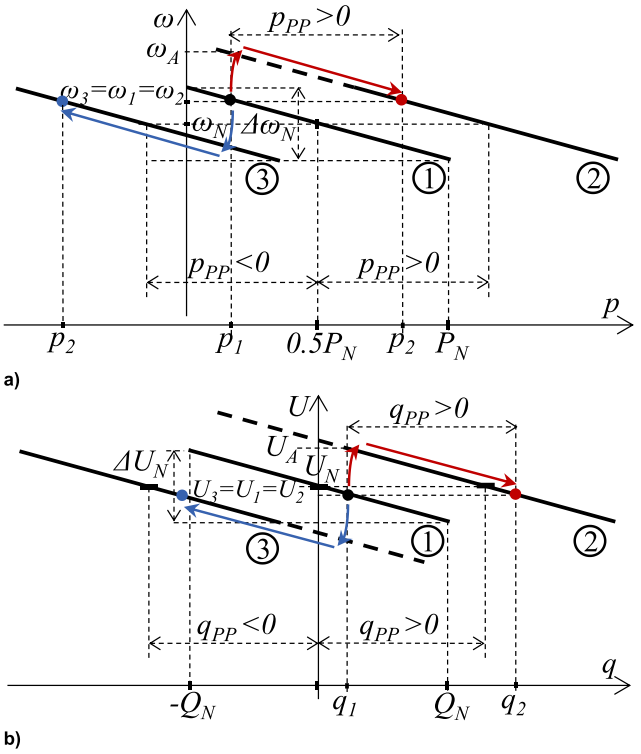


**FIGURE 3.** Droop control: a) $p$–$\omega$ characteristic, b) $q$–$u$ characteristic.

Without peer-to-peer terms, $p_{PP}$ and $q_{PP}$, expressions (1), (2), and (3) would constitute the conventional droop controller (characteristics denoted "1" in Fig. 3.a and Fig. 3.b, respectively). It is expected that the conventional part of the proposed droop control law would effectively suppress the interfering instances in the MG system, such as ( [8], [18]):

- deviations of the steady-state voltage magnitudes along the MG line, where in conjunction with the secondary control (via $dU$ term), it would make PUs cooperatively contribute to the regulation of the PCC voltage to the nominal level.
- deviations of the MG frequency from the nominal value, where in conjunction with the secondary control (via $d\omega$ term), it would make PUs cooperatively restore the frequency to the nominal value.
- the delay in communication between the contractees, volatile power consumption of the uncontrollable loads, volatile power generation of the renewable energy generation and volatile consumption and generation of the disrupting units, which would be dealt with by all neighboring PUs cooperative reaction.

It should be noted, that the PU's power capacity assigned to the conventional droop control come at the expense of the reduced power trading prospects. However, in the case of communication link disruptions, or even its complete failure, the proposed control strategy reduces to conventional droop control when it keeps providing uninterrupted operation of all individual units without any jeopardy with respect to the stability of the MG.

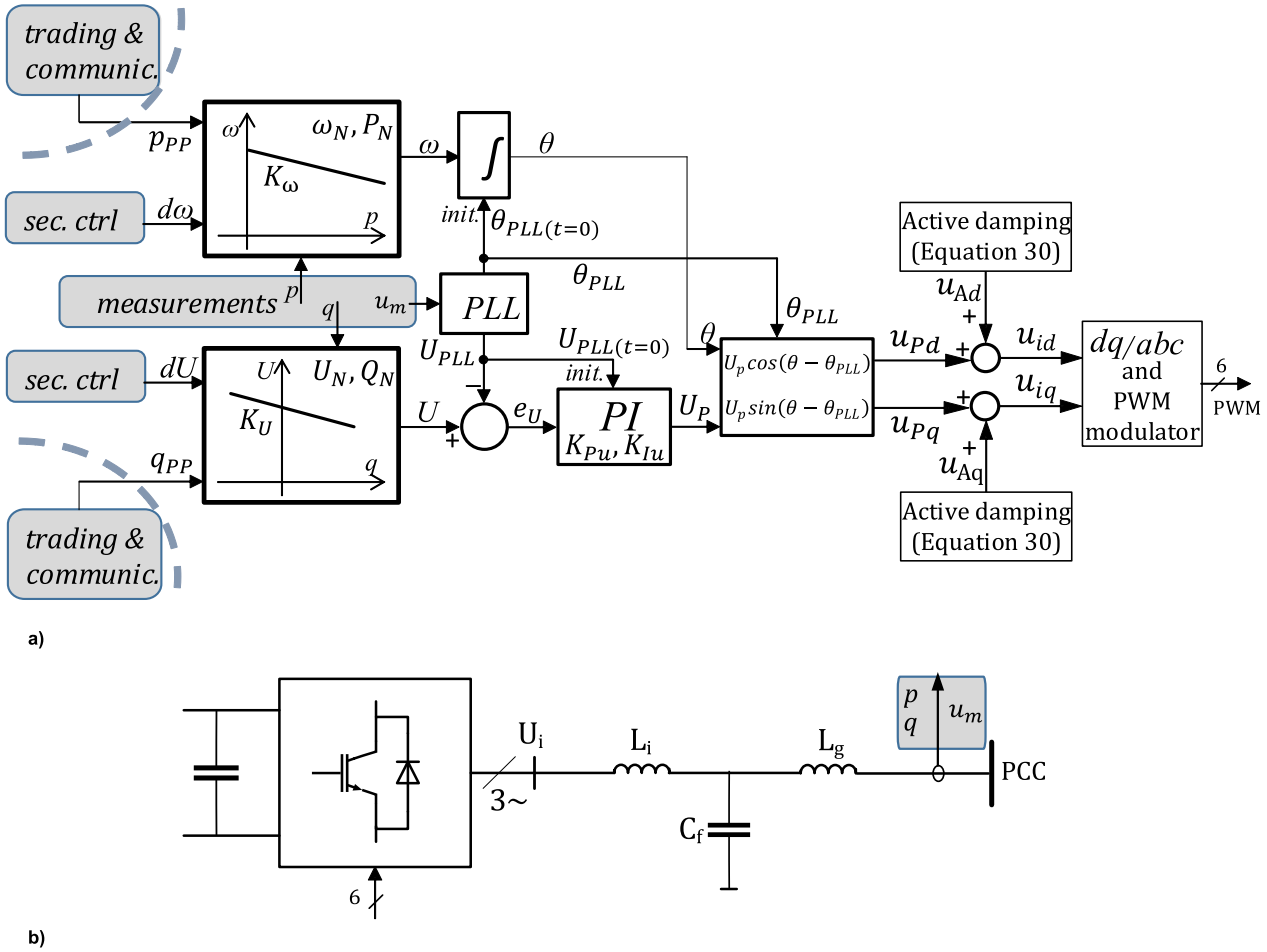


**FIGURE 4.** Prosumer unit: a) control structure and b) power stage with LCL filter.

The introduction of the peer-to-peer contracted instantaneous active and reactive power terms, $p_{PP}$ and $q_{PP}$ in Expressions (1) and (2), should produce corresponding power flows exclusively between the contractees. The $p_{PP}$ and $q_{PP}$ terms shift droop characteristics horizontally, as shown in Fig. 3. The characteristics denoted "2" correspond to a PU bound to deliver the contracted active power ($p_{PP} > 0$) i.e. reactive power ($q_{PP} > 0$) and characteristics denoted "3" correspond to the PU bound to receive the active power ($p_{PP} < 0$) or the reactive power ($q_{PP} < 0$). Followed by almost simultaneous changes in the active and/or reactive power at the contractees' power nods, corresponding assignments of $p_{PP}$ and $q_{PP}$ have the following implications on the MG steady-state and transitional periods (regarding the implementation of expressions (4) and (5)):

- The new steady-state angular frequency, $\omega$, will remain at the previous level because the active power throughput of the other PUs (other than those two that are exchanging $p_{PP}$) will remain unaltered ($\omega_1$=$\omega_2$ in Fig. 3.a).
- At the start of the transitional period after $p_{PP} > 0$ step change, $\omega$ of the grid-tie converter output frequency will jump from $\omega_1$ to $\omega_A$ and then slide down the slope of the $p$-$\omega$ characteristic back to $\omega_2$=$\omega_1$ (as indicated in Fig. 3.a). The integral of the transition in $\omega$ (see Expression (4)) will eventually provide a new value of the PU's power angle (the angular difference between the PU voltage and the PCC voltage.
- the new steady-state voltage level at the PCC will remain at the previous level because the reactive power throughput of other PUs (other than those two that are exchanging $q_{PP}$) will remain unaltered ($U_1$=$U_2$ in Fig. 3.b).
- At the start of the transitional period after $q_{PP} > 0$ step change, the reference value of the PU's output voltage, $U$, will jump from $U_1$ to $U_A$ and then slide down the slope of the $q$-$u$ characteristic back to $U_2$=$U_1$ (as indicated in Fig. 3.b). The integral of the transition in $U$ (see Expression (5)) will eventually provide a new value of the PU's output voltage, $u_P$, corresponding to the set value of $q_{PP}$ and the voltage drop across the coupling filter inductance.
- The responses for negative values of the contracted powers ($p_{PP} < 0$ and $q_{PP} < 0$) are analogous. The feature of acquiring the amount of active and/or reactive power is

the compulsory feature of PUs, something that does not exist with conventional distribution generation units.

The core of the proposed control algorithm is essentially a coupling of conventional droop control and feed-forward action. It is a well-known fact that feed-forward control signals, if they are external to the control-loop, do not affect stability of linear control systems. Intuitively, the same holds for mildly non-linear systems and even mutualy coupled feed-forward actions operating on significantly slower time-scale. Consequently, the stability of the microgrid will be determined by the droop stability. Relationship between droop parameters, system parameters and stability margins can be identified, using qualitative analysis and small-signal techniques [30].

Although the communication layer was not in the focus of this study, its scalability will be briefly discussed here. One of the crucial features of the P2P framework is that communication load of any of the incorporated units is independent of the total number of units. It is because the number of the contracts that it makes, does not increase with the increase of actual size of the MG. Also, the total communicated data traffic grows with less than linear scale because the coordination and communication overhead is limited by the outdegree of the communication graph, which is equal to the maximal number of bilateral contracts that an individual prosumer may have [31]. This is in a contrast with centralized and distributed MG setups where either central unit data loading increases linearly or each unit's data loading increases linearly.

Another critical feature of the system is the communication latency. There are already solutions that can answer to the highest requirements. Namely, according to the 5G network - 3GPP standardization body [32], it is required that mission-critical services, such as factory automation and autonomous driving, are provided with Radio Access Networks that guaranty latency lower than 10 ms measured at application layer with data bit rates of tens of Mbps. This Ultra Reliable Low Latency Communication (URLLC) is the key feature of 5G.

## III. PROSUMER UNIT'S INTERFACE FOR LIMITED VOLTAGE HARMONICS DISTORTION

PU's interface is to be designed based on the voltage harmonic distortion limit that the PU may generate at the PCC and neighboring MG nodes. Namely, while PUs are sinking or sourcing current in the on-grid mode and should therefore adhere to the current distortion limitations, PUs form the MG voltage in the off-grid mode and are therefore responsible for its quality. In the surrounding MG, especially in off-grid operation, utilization of the high-order filters, LC or LCL, is necessity because the sinusoidal output voltage is required. However, only the LCL filter provides the required decoupling toward the neighboring units (that could be connected at the same PCC or in its vicinity), and lowers current and voltage control sensitivity to the variations in the equivalent grid impedance due to the changes in the MG topology and the number and type of the connected loads and sources.

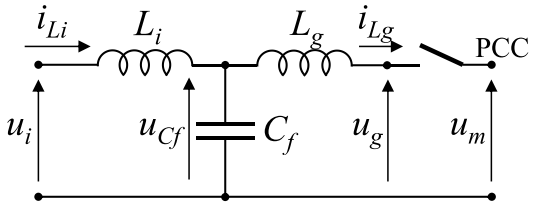


**FIGURE 5.** LCL coupling filter.

### A. DESIGN OF THE COUPLING LCL FILTER

Following the previously noted, the process of designing filter parameters (Fig. 5) is governed by three main objectives: 1) to provide the grid current high-order harmonics attenuation in the on-grid mode; 2) to limit the voltage distortion at the PCC below the limit values and 3) to attain the maximal dynamic responsiveness of the filter.

The third objective directs the selection of the inductances, $L_i$ and $L_g$, and capacitance, $C_f$, toward the lowest energy storage individually and cumulatively so that the control of their states requires the lowest control effort. Accordingly, $L_i$, $L_g$, and $C_f$, values should be set as minimal as possible, and their corresponding energies, given in (6), should be approximately equal.

$$E_{Li} = \frac{1}{2} \cdot L_i \cdot I_n^2, E_{Lg} = \frac{1}{2} \cdot L_g \cdot I_n^2, E_{Cf} = \frac{1}{2} \cdot C_f \cdot U_{Pn}^2 \quad (6)$$

It follows that the total inductance should be equally split between $L_i$ and $L_g$, that is, $L_i = L_g$. Arguably, this is the most common approach in practice as it provides for the minimal total inductance, minimal voltage drop, highest dynamical performance, minimal required capacitance, and minimal reactive power consumption [27], [28]. This condition together with the set of expressions (6) determines the relation between the inductances' and $C_f$ values.

The first and second design objectives are incorporated in an iterative two-step process. In the first step, the filter's cut-off frequency has to be chosen. Considering introductory discussion on limited voltage and current harmonics' distortion, there are actually two resonant frequencies to be chosen: resonant frequency of voltage output – to – voltage input transfer function, $U_m(j\omega)/U_i(j\omega)$, designated by $\omega_{U\_res}$, and resonant frequency of current output – to – voltage input transfer function, $I_m(j\omega)/U_i(j\omega)$, designated by $\omega_{I\_res}$. The first one, $\omega_{U\_res}$ – in further text called voltage cut-off frequency, is calculated when the filter output is in disconnected state (with switch opened in Fig. 5):

$$\omega_{U\_res} = \sqrt{\frac{1}{L_i \cdot C_f}}. \quad (7)$$

The second one, $\omega_{I\_res}$ – in further text referred as current cut-off frequency, is calculated when the filter output is in the short-circuit state. This corresponds to the on-grid state of the PU, i.e. when high-order current harmonics are

short-circuited through the mains voltage:

$$\omega_{I\_res} = \sqrt{\frac{L_i + L_g}{L_i \cdot C_f \cdot L_g}}. \tag{8}$$

Although, both expressions (7) and (8), neglect influence of the MG line parameters and are approximate, the further analysis of the voltage and current harmonics will show that given filter output states, namely, open-circuit and on-grid, are the most critical cases, respectively. Considering the choice $L_i = L_g = L$, expressions (7) and (8) become:

$$\omega_{I\_res} = \sqrt{\frac{2}{L \cdot C_f}} = \sqrt{2} \cdot \omega_{U\_res}. \tag{9}$$

Probing for the appropriate value of $\omega_{I\_res}$ should start from its highest limit value, which is $\omega_{sw}/2$ [27].

In the second step, high-order current and voltage harmonic attenuation are determined and evaluated for compliance with a given harmonic distortion standard. The procedure is completed when, for the obtained LCL parameters, the high-order current and voltage harmonic distortion fall below the requested levels.

In the on-grid mode, the power quality standards set the maximal current distortion level (*HDI*). For example, according to IEEE 519-2014, in a relatively weak distribution grid with $I_{SC}/I_N < 20$ (where $I_N$ is the nominal PU current and $I_{SC}$ is the short-circuit current at the PCC), the high-order harmonic current distortion for $h \geq 35$ (where $h$ is the order of the harmonic) is limited to $0.3\%\, I_N$. However, there are no corresponding norms for assessing the influence of PU on the MG in the off-grid mode [33], [34].

Here, the task of the coupling filter is to attenuate voltage high-order switching harmonics so that the total harmonic voltage distortion *(THDU)* at each MG node is inside prescribed limits. The influence of one PU can be determined by comparing its Thevenin equivalent, including the equivalent voltage, $\underline{U}_t$, and impedance, $\underline{Z}_t$, as given in Equation (10), to the equivalent impedance of the rest of MG (Fig. 6).

$$\begin{aligned} \underline{U}_t &= \frac{\underline{Z}_{Cf}}{\underline{Z}_{Cf}+\underline{Z}_{Li}} \cdot \underline{U}_i = \frac{1}{1-\omega^2 \cdot L_i \cdot C_f} \cdot \underline{U}_i \\ \underline{Z}_t &= \underline{Z}_{Lg} + \frac{\underline{Z}_{Cf} \cdot \underline{Z}_{Li}}{\underline{Z}_{Cf}+\underline{Z}_{Li}} = j\omega \cdot \frac{L_i + L_g - \omega^2 \cdot L_i \cdot L_g \cdot C_f}{1-\omega^2 \cdot L_i \cdot C_f} \end{aligned} \tag{10}$$

where $\underline{U}_i$ is the grid-tie converter output voltage, $\underline{Z}_{Li} = j\omega \cdot L_i$, $\underline{Z}_{Lg} = j\omega \cdot L_g$, $\underline{Z}_{Cf} = \left(j\omega \cdot C_f\right)^{-1}$.

As perceived from the PU side of the PCC, the MG setup can span the following three forms:

- MG setup featuring the pronounced presence of neighboring PUs or other units that have a grid-tie converter at its front end (e.g., DGs, active front-end motor drives, STATCOMs). In the following, it is referred to as "*active PCC.* "
- MG setup in which the PCC's neighboring area of concern hosts only passive loads (different heaters, AC motors, and incandescent lighting). In the following, it is referred to as "*passive PCC.* "

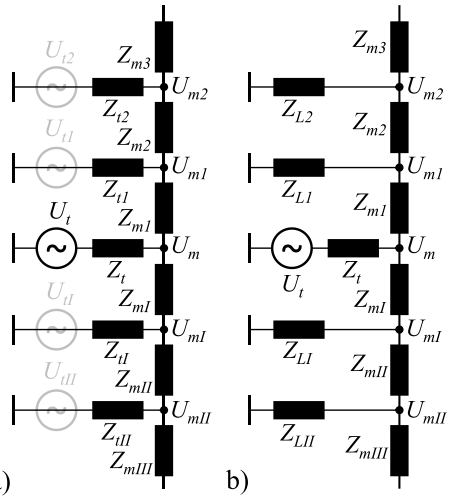


**FIGURE 6.** Two high-frequency harmonic models of the MG from the PU perspective: a) *active* PCC, b) *passive* PCC.

- MG setup hosting the pronounced presence of loads with a diode rectifier and a filter DC capacitor at their main inputs. In the following, it is referred to as "*rectifiers' PCC*".

At the *active PCC*, neighboring units add a level of harmonic voltage distortion to the observed PCC increasing the level of the total voltage distortion. Their influence depends on their output voltage harmonic spectrum and the distance from the PCC. To ensure that the total voltage distortion limit value is not exceeded regardless of the number of units, the following critical conditions need to be considered:

1. Each unit must adhere to the universal power quality standard regarding the individual voltage distortion.
2. The most critical MG parameters need to be considered, causing maximal voltage distortion in the grid nodes.
3. The possible harmonic cancelation between the units will be ruled out.

The first condition indicates that the filtering capacities of each unit's coupling filter are quite similar and, correspondingly, that their Thevenin impedances are comparable (note that the Thevenin impedances of the LCL filters designed in [27], [28], and [29] differ by less than 20%). The second critical condition concerns the spatial distribution of the units along the radial MG line (Fig. 6.a), that is, the distribution of the line impedances $Z_m$ between neighboring PCCs. There are two opposite cases to be considered: a) the units are closely connected, meaning $Z_{m1} \approx Z_{mI} \approx Z_{m2} \approx Z_{mII} \approx \ldots \approx Z_m \approx 0$, and b) the units are equally distributed along the weak MG line $Z_{m1} \approx Z_{mI} \approx Z_{m2} \approx Z_{mII} \approx \ldots \approx Z_m$. The maximal value of $Z_m$, in all practical cases [8], does not exceed $Z_{Lg}$ and, correspondingly, $Z_t$. (It should be noted that $L_g$ dominates $Z_t$ in (10) as $C_f$ essentially bypasses $Z_i$ at frequencies around and above $f_{sw}$, that is, $Z_t \approx j \cdot \omega \cdot L_g$.) Therefore, to maximize $Z_m$ influence, $Z_m$ would be overrated and set equal to $Z_t$, that is, $Z_{m1} = Z_{mI} = Z_{m2} = Z_{mII} = \ldots = Z_m = Z_t$. Finally, according to the third condition, the *THDU* at each

of the PCCs has to be calculated as the cumulative impact of all PU harmonic components, $U_{t(h)}$. This gives way to the superposition of individual harmonic voltage components, $U_{t(h)}$, $U_{t1(h)}$, $U_{tI(h)}$, $U_{t2(h)}$, $U_{tII(h)}$,... as indicated in Fig.6.a). Based on the PUs' Thevenin equivalents ($U_t$ and $Z_t$) and MG equivalent impedances at particular nodes, the individual harmonic voltages can be calculated along the line, $U_{m(h)}$, $U_{m1(h)}$, $U_{mI(h)}$, $U_{m2(h)}$, $U_{mII(h)}$,...considering that the order of harmonics, $h$, is different for all PUs, i.e. their switching frequencies are not synchronized.

*Case 1*: THDU at active PCC with $Z_m$=0

Having $N$ units connected in the common PCC, each Thevenin voltage harmonic component, $U_{t(h)}$, translates into $U_{m(h)}$ as follows:

$$\left|\underline{U}_{m(h)}\right| = \frac{1}{N+1} \cdot \left|\underline{U}_{t(h)}\right| \tag{11}$$

The corresponding *THDU* amounts to:

$$THDU = \frac{1}{(N+1)\cdot U_1} \sqrt{\sum_h \left|\underline{U}_{m(h)}\right|^2 + \sum_h \left|\underline{U}_{m1(h)}\right|^2 + \sum_h \left|\underline{U}_{mI(h)}\right|^2 + \ldots} < \frac{1}{(N+1)\cdot U_1} \cdot \sum_{x=1}^{N} \sqrt{\sum_h \left|\underline{U}_{mx(h)}\right|^2} \approx THDU_{avg} \tag{12}$$

It follows that the *THDU* at the given MG section corresponds to the *THDU* of an average PU, $THDU_{avg}$, that is, the *THDU* in the MG node will be limited to the designated value if the Thevenin voltage distortion of each PU is limited accordingly.

*Case 2*: THDU at active PCC with $Z_m = Z_t$

With $N$ units connected to each side of the observed PCC, the Thevenin voltage harmonic component, $U_{t(h)}$, translates into the neighboring nodes (*m, m1, mI, m2, mII, ...mN*) as follows:

$$\begin{aligned}
\left|\underline{U}_{m(h)}\right| &= \frac{1+K_N}{3+K_N} \cdot \left|\underline{U}_{t(h)}\right|, \\
\left|\underline{U}_{m1(h)}\right| &= \left|\underline{U}_{mI(h)}\right| = \frac{K_N}{1+K_N} \cdot \left|\underline{U}_{m(h)}\right| \\
\left|\underline{U}_{m2(h)}\right| &= \left|\underline{U}_{mI(h)}\right| = \frac{K_{N-1}}{1+K_{N-1}} \cdot \left|\underline{U}_{m1(h)}\right|, \ldots, \\
\left|\underline{U}_{mK(h)}\right| &= \left|\underline{U}_{mk(h)}\right| = \frac{K_{(N-k+1)}}{1+K_{(N-k+1)}} \cdot \left|\underline{U}_{m(k-1)(h)}\right|, \ldots, \\
\left|\underline{U}_{mN(h)}\right| &= \left|\underline{U}_{mn(h)}\right| = \frac{K_1}{1+K_1} \cdot \left|\underline{U}_{m(N-1)(h)}\right|
\end{aligned} \tag{13}$$

where $K_i$ is:

$$K_i = \frac{A_i \cdot i - C_i}{B_i \cdot i - D_i}, \tag{14}$$

and coefficients $A_i$, $B_i$, $C_i$, and Di can be calculated algorithmically as

$$\begin{aligned}
A_i &= A_{i-1} + B_{i-1}; A_1 = 1 \\
B_i &= A_i + B_{i-1}; B_1 = 1 \\
C_i &= A_i + C_{i-1} + D_{i-1}; C_1 = 0 \\
D_i &= C_i + B_{i-1} + D_{i-1}; D_1 = -1.
\end{aligned} \tag{15}$$

It happens that $A_i$ and $B_i$ are elements of Fibonacci sequence and as such they can be calculated explicitly:

$$A_i = Fib(2\cdot i - 3), B_i = Fib(2\cdot i - 2), \tag{16}$$

where $Fib\,(j) = \frac{\varphi^j - (-\varphi)^{-j}}{\sqrt{5}}$, $\varphi = \frac{1+\sqrt{5}}{2}$. The obtained row of the voltage magnitudes shows a steeply growing attenuation of the harmonic source voltage $U_t$ as moving downstream from the origin:

$$\begin{aligned}
\left|\underline{U}_{m(h)}\right| &= 0.447 \cdot \left|\underline{U}_{t(h)}\right|, \left|\underline{U}_{m1(h)}\right| = 0.171 \cdot \left|\underline{U}_{t(h)}\right|, \\
\left|\underline{U}_{m2(h)}\right| &= 0.065 \cdot \left|\underline{U}_{t(h)}\right|, \left|\underline{U}_{m3(h)}\right| = 0.025 \cdot \left|\underline{U}_{t(h)}\right|, \\
\left|\underline{U}_{m4(h)}\right| &= 0.010 \cdot \left|\underline{U}_{t(h)}\right|, \ldots
\end{aligned} \tag{17}$$

It should be noted that attenuation values do not depend on harmonic frequency. Still, the Thevenin voltage, $U_t$, decreases with a quadratic function of $\omega$, as obtained with (10). According to (17), the *THDU* in the PCC should consider up to three neighboring nodes on both sides of the PCC:

$$\begin{aligned}
&THDU \\
&= \frac{1}{U_1} \cdot \sqrt{\begin{aligned}&0.447^2 \cdot \textstyle\sum_h \left|\underline{U}_{m(h)}\right|^2 + 2\cdot 0.171^2 \cdot \sum_h \left|\underline{U}_{m1(h)}\right|^2 \\ &+ 2\cdot 0.065^2 \cdot \textstyle\sum_h \left|\underline{U}_{m2(h)}\right|^2 + \\ &+ 2\cdot 0.025^2 \cdot \textstyle\sum_h \left|\underline{U}_{m3(h)}\right|^2\end{aligned}} \\
&\approx 0.52 \cdot THDU_{avg}
\end{aligned} \tag{18}$$

where $THDU_{avg}$ corresponds to the *THDU* of an average PU.

Based on (12) and (18) and the linearity of the *active PCC* circuit shown in Fig. 6.a, the important conclusion is that for any realistic ratio of the distribution line impedances, $Z_m$, to the PU's Thevenin impedance $Z_t$, the *THDU* in any of the grid nodes would not exceed the *THDU* of any of the neighboring PUs in their disconnected state.

*Case 3:* THDU at passive PCC

Figure 6.b. shows a PU facing passive loads in the neighboring nodes, i.e. *passive* PCC. Although each of the passive loads is modeled by the impedances, $Z_{Li}$, it should be noted that it may comprise a voltage source at the MG frequency, $\omega \approx \omega_N$, (e.g. induced electromagnetic forces). However, this voltage source appears as the zero voltage source in the high-frequency harmonic model. Line impedances, $Z_{mi}$, and load impedances, $Z_{Li}$, together make the PCC equivalent impedance, $Z_{eq}$, that, with the Thevenin impedance, $Z_t$, form the PU's Thevenin voltage divider:

$$\underline{U}_{m(h)} = \frac{\underline{Z}_{eq}}{\underline{Z}_t + \underline{Z}_{eq}} \cdot \underline{U}_{t(h)}. \tag{19}$$

Only the predominantly inductive $Z_{eq}$ forms the voltage divider with $Z_t$, because $Z_t$ has inductive character according

to (10) and $Z_t \approx j{\cdot}\omega{\cdot}L_g$ for $\omega \geq \omega_{sw}$:

$$\underline{U}_{m(h)} \approx \frac{j\omega L_{eq}}{j\omega L_g + j\omega L_{eq}} \cdot \underline{U}_{t(h)} = \frac{L_{eq}}{L_g + L_{eq}} \cdot \underline{U}_{t(h)}. \quad (20)$$

According to (20), the highest *THDU* is obtained at light loading [35], that is, $L_{eq} \gg L_g$. This leads to $\underline{U}_{m(h)} \approx \underline{U}_{t(h)}$ and $THDU{\approx}THDU_{avg}$. It should be noted that the *THDU* in the light loading condition corresponds to the *THDU* of the PU output voltage in its disconnected state (with the switch opened in Fig. 5).

A similar impact has a resistive $Z_{eq}$ ($Z_{eq} = R_{eq}$). The combination of the resistance and reactance $L_g$ produces a somewhat nonlinear voltage division function at (19); however, concerning the *THDU*, their critical ratio corresponds to the light loading condition, $R_{eq} \gg |j{\cdot}\omega{\cdot}L_g|$, leading to $THDU{\approx}THDU_{avg}$. The predominantly capacitive $Z_{eq}$ ($Z_{eq} \approx 1/j{\cdot}\omega{\cdot}C_{eq}$) forms an additional voltage filtering branch, further reducing the high-order harmonics $U_{m(h)}$:

$$\underline{U}_{m(h)} \approx \frac{1}{1 - \omega^2 \cdot L_g \cdot C_{eq}} \cdot \underline{U}_{t(h)}. \quad (21)$$

Therefore, the capacitive $Z_{eq}$ leads to the comparatively lowest *THDU*.

*Case 4*: THDU at rectifiers' PCC

The harmonic model of the rectifier with the filter DC capacitor consists of shunt-connected low-order harmonic current sources at $h = 5, 7, 11, \ldots$ Injecting the current distortion, these loads would, from their side, cause the harmonic voltage distortion only if neighboring PUs are not capable of sinking these currents, i.e behaving as active filters (e.g. [36]). The active filtering capabilities of a PU do not directly impact the design requirements of the coupling filter because there should be a fair frequency gap between the corresponding frequency bands. Therefore, in the range of the switching frequency spectrum, a load with a rectifier at the input terminals appears as an open circuit. Therefore, from the perspective of the PU's coupling filter performance, this type of load does not have an impact on $U_{m(h)}$, that is, $\underline{U}_{m(h)} \approx \underline{U}_{t(h)}$, nor on the *THDU*, that is, $THDU{\approx}THDU_{avg}$.

Based on the presented study using terminal MG harmonic models, the PU's *THDU* performance facing a generic mixture of the *active* and *passive* elements at the PCC can be estimated as follows:

- The presence of *passive* elements among the *active* elements favorably affects the *THDU* in two aspects: the passive elements lower $Z_{eq}$ and they do not introduce additional voltage distortion.
- The presence of the *active* elements among the *passives* favorably affects the *THDU*: although they introduce harmonic distortion, by lowering $Z_{eq}$, active elements move the PCC away from the light-loading condition, which is critical in the predominantly passive PCC.
- The presence of loads with the rectifier at its inputs does not affect the *THDU* at the PCC.

Finally, it can be concluded that the *THDU* in each MG node will be limited according to a standard if each PU in the disconnected state generates the *THDU* below the given limit value.

### B. CORRELATION BETWEEN PI'S THDU AND THDI PERFORMANCE

Unlike *THDU* which is comparatively maximal in disconnected state of a PU, i.e. when switch from Fig. 5 is opened, *THDI* is maximal when there is a sort of a short-circuit for LCL filter's high-order harmonics at PCC. The closest situation to that is in the on-grid mode of MG when the grid behaves as a voltage source at the fundamental frequency but as a short-circuit for higher current harmonic components. Neglecting the MG line impedance and the impedance of the grid itself, maximal harmonic currents' magnitudes are obtained as:

$$\left|I_{(h)}\right| = \frac{1}{\left|Z_{t(h)}\right|} \cdot \left|U_{t(h)}\right|. \quad (22)$$

It can be seen that current harmonics' attenuation is higher than the voltage harmonics' attenuation by the factor of $\left|Z_{t(h)}\right| / \left|Z_{t(1)}\right|$. Correspondingly, the ratio between individual current harmonic distortion, $HDI_{(h)}$, and individual voltage harmonic distortion, $HDU_{(h)}$, meets the following:

$$HDI_{(h)} = \frac{\left|Z_{t(1)}\right|}{\left|Z_{t(h)}\right|} \cdot HDU_{(h)}. \quad (23)$$

To determine the approximate rating of this factor, based on (10), $\left|Z_{t(h)}\right|$ can be expressed as:

$$\underline{Z}_{t(h)} = j \cdot 2 \cdot h \cdot \omega_1 \cdot L \cdot \frac{1 - h^2 \cdot \frac{\omega_1^2}{\omega_{I\_res}^2}}{1 - 2 \cdot h^2 \cdot \frac{\omega_1^2}{\omega_{I\_res}^2}}, \quad (24)$$

where, according to the first design objective, $L_i = L_g = L$, according to (7) is $\omega_{I\_res} = \sqrt{2/(C_f \cdot L)}$, and $\omega = h \cdot \omega_1$. Employing any of the PWM schemes for output voltage generation, high-order harmonic spectrum is always dominated by switching harmonics around $\omega_{sw}$, $2{\cdot}\omega_{sw}$, $3{\cdot}\omega_{sw}$, …, etc. At corresponding frequencies, their order in the spectrum, $h$, is higher than $\omega_{I\_res}/\omega_1$ by more than two times (usually $\omega_{I\_res} = \omega_{SW}/(2 \div 4)$). Hence, the particle in (24) can be approximated by 1/2 (for $\omega_{I\_res} = \omega_{SW}/2$ it is 3/7; for $\omega_{I\_res} = \omega_{SW}/3$ it is 8/17, etc.) giving:

$$\underline{Z}_{t(h)} \approx j \cdot h \cdot \omega_1 \cdot L, \quad (25)$$

On the other hand, for $h{=}1$ and acknowledging that $\omega_{I\_res} \gg \omega_1$:

$$\underline{Z}_{t(1)} \approx j \cdot 2 \cdot \omega_1 \cdot L, \quad (26)$$

Therefore, for the harmonic spectrum caused by the converter switching, $HDI_{(h)}$ to $HDU_{(h)}$ ratio is approximately equal to:

$$HDI_{(h)} \approx \frac{2}{h} \cdot HDU_{(h)} \quad (27)$$

This indicates that for a PU having LCL filter as interface towards the MG, *THDU* demands in the off-grid mode are

much more critical to fulfill then *THDI* demands in the on-grid mode. *THDI* performance in the MGs' off-grid mode has not be analyzed analytically here. Still, comparatively higher total impedance of the combined PUs and/or other loads inside the MG itself, would produce even higher current harmonics' attenuation in comparison to the *THDI* in on-grid mode. The simulation results given in the next section clearly confirm the conclusions of this study.

### C. EXAMPLE OF THE LCL COUPLING FILTER DESIGN

The MG nominal voltage, $U_N$, and nominal angular frequency, $\omega_N$, are given in Table 1. The PU's nominal apparent power, $S_N$, and the switching frequency $f_{SW}$ correspond to the prosumer unit $PU_1$ given in Tables 1 and 2, respectively. The initial probing value for the coupling filter voltage cut-off frequency is $f_{U\_res} = 2{,}6$ kHz. The value provides, on one hand, enough distance from the switching frequency, $f_{SW}$, and, on the other hand, leaves enough room for the primary controller to attain a high dynamical response. Adding the objective of having equal energy flows through the filter inductances and capacitance, the following filter parameters are obtained: $L_i$=$L_g$=1,5 mH and $C_f$=4,7 $\mu$F; (according to (6): $E_{Li}$=$E_{Lg}$=8,3 J, $E_{Cf}$=8,5 J).

According to the presented analysis, the *THDU* is measured at the PU terminals in its disconnected state. The recorded value of 1.3% is well below the IEEE 519-2014 standard *THDU* limit of 5%. Therefore, no additional iterations (that would assume lower $f_{U\_res}$) are required in the given example. Verification of the obtained PU performance regarding the *THDU* is done by micro-grid simulation in the off-grid mode and presented in Chapter IV.

To confirm the findings of *THDU* vs *THDI* analysis, the individual current harmonic distortion (*HDI*), that corresponding PU injects into the PCC, was tracked in the on-grid mode of operation. The fundamental current harmonic, $I_{(1)}$, was set to the nominal value (105 [$A^{RMS}$]). The measurement results show the predominance of switching frequency sidebands amounting to $HDI_{(200)}$=0.055%. The *HDI* level is well below the limit of 0.3% set by IEEE 519-2014.

### D. ACTIVE DAMPING CONTROL OF THE COUPLING FILTER

The design of the LCL filter is tightly linked to the task of attaining the needed level of stability, that is, the damping of its inherent resonance. There are two approaches to filter damping: passive approach and active approach, where active damping is usually preferred owing to the efficiency issues of the passive concept. Active damping can be implemented by the grid-tie converter utilizing a dedicated control algorithm, which may be hardware-backed by including additional sensors of inductors currents and/or capacitor voltages. The active damping algorithm has to tackle possible changes in the grid parameters and grid topology and possible influence of the neighboring units. It should be noted that all these unknowns are pronounced in the MG environment. There is almost a direct correlation between the active damping susceptibility to these influences and the number of measured system variables. The simplest sensory setup includes measurements of the currents of the converter-side inductances and grid voltages. Here, active damping can be achieved by sophisticated tuning of the grid-tie converter's modulation signals [37]. Solutions aiming at higher robustness are supplemented by the measurements and control of the other filter state variables: in [29], the filter capacitor voltages are measured and used to form the lead-leg inner control loop; in [28], capacitor currents are used in combination with the lead-lag compensator; in [38], the grid currents are measured to apply the virtual damping resistor concept, in [39] the high active damping robustness is retained even under the considerable variations in the filter parameters utilizing the grid current measurement and the application of the multiple-input-multiple-output (MIMO) controller, in [40] all state variables are measured, including the converter-side and grid-side inductances' currents and capacitors' voltages, to form the state-feedback compensator and thus attain the stability margin and, simultaneously, the current limitation even under transients and faults. It is possible to estimate some of the control variables by employing a state estimator (e.g., Kalman filter [34]) and thus relax the filter hardware from some of the measurements.

This study considers the most generic approach in which all filter state variables are measured. It has served as a basis for the active damping algorithm design that provides the maximal dynamical performance and thus decouples it as much as possible from the other control objectives and the MG system dynamics, making the wide-scale system analysis easier to perceive and interpret. Here, the MIMO controller was employed and its parameters were designed to: 1. attain active damping, and 2. attain flawless synchronization of the PU to the PCC voltage.

Expression (28) is a state-space representation of the mathematical model of the LCL filter from Fig. 5, expressed in grid-voltage-oriented $dq$ coordinates. The first three rows relate the coupling filter state variables, $\underline{i}_{Li} = \left[\, i_{Lid} \;\; i_{Liq} \,\right]^T$, $\underline{u}_{Cf} = \left[\, u_{Cfd} \;\; u_{Cfq} \,\right]^T$, $\underline{i}_{Lg} = \left[\, i_{Lgd} \;\; i_{Lgq} \,\right]^T$ with the converter output voltage $\underline{u}_i = \left[\, u_{id} \;\; u_{iq} \,\right]^T$ and the filter output voltage $\underline{u}_g = \left[\, u_{gd} \;\; u_{gq} \,\right]^T$,

$$\frac{d}{dt}\begin{bmatrix} \underline{i}_{Li} \\ \underline{u}_{Cf} \\ \underline{i}_{Lg} \\ \underline{u}_S \end{bmatrix} = \begin{bmatrix} \omega_g \cdot \underline{\boldsymbol{J}} & -\frac{1}{L_i}\cdot \underline{\boldsymbol{I}} & \underline{0} & \underline{0} \\ \frac{1}{C_f}\cdot \underline{\boldsymbol{I}} & \omega_g \cdot \underline{\boldsymbol{J}} & -\frac{1}{C_f}\cdot \underline{\boldsymbol{I}} & \underline{0} \\ \underline{0} & \frac{1}{L_g}\cdot \underline{\boldsymbol{I}} & \omega_g \cdot \underline{\boldsymbol{J}} & \underline{0} \\ \underline{0} & \underline{\boldsymbol{I}} & \underline{0} & \underline{0} \end{bmatrix} \cdot \begin{bmatrix} \underline{i}_{Li} \\ \underline{u}_{Cf} \\ \underline{i}_{Lg} \\ \underline{u}_S \end{bmatrix} + \begin{bmatrix} \frac{1}{L_i}\cdot \underline{\boldsymbol{I}} \\ \underline{0} \\ \underline{0} \\ \underline{0} \end{bmatrix} \cdot \underline{u}_i + \begin{bmatrix} \underline{0} \\ \underline{0} \\ -\frac{1}{L_g}\cdot \underline{\boldsymbol{I}} \\ -\underline{\boldsymbol{I}} \end{bmatrix} \cdot \underline{u}_g$$

$$= \underline{A} \cdot \begin{bmatrix} \underline{i}_{Li} \\ \underline{u}_{Cf} \\ \underline{i}_{Lg} \\ \underline{u}_S \end{bmatrix} + \underline{B}_i \cdot \underline{u}_{iA} + \underline{B}_g \cdot \underline{u}_g, \tag{28}$$

where $\underline{\boldsymbol{I}}$ is the identity matrix $\underline{\boldsymbol{I}} = \begin{bmatrix} 1 & 0 \\ 0 & 1 \end{bmatrix}$, $\underline{\boldsymbol{J}}$ is the anti-diagonal matrix $\underline{\boldsymbol{J}} = \begin{bmatrix} 0 & 1 \\ -1 & 0 \end{bmatrix}$ and $\omega_g$ is the grid angular frequency, and, at the same time, the angular speed of the $dq$ coordinate system. The fourth row of the equation corresponds to the model of the synchronizing error integrator. As shown in Fig. 7, the synchronizing voltage error $(\underline{u}_{Cf} - \underline{u}_g)$ integrator adds two extra state variables $\underline{u}_S = \begin{bmatrix} u_{Sd} & u_{Sq} \end{bmatrix}^T$:

$$\frac{d}{dt}\underline{u}_S = \underline{u}_{Cf} - \underline{u}_g. \tag{29}$$

In the PU disconnected state, the capacitor voltage $\underline{u}_{Cf}$ is used as an estimate of the PU terminal voltage, which is valid because $\underline{i}_{Lg}$=0. After the PU connection, the terminal voltage becomes equal to $\underline{u}_g$, acknowledged by bypassing the integrators' inputs to zero (controlled by the "*synch*" signal; see Fig. 7).

Model (17) has eight characteristic poles: $s_{1\div4} = \pm j(\omega_{res} \pm \omega_g)$, $s_{5,6} = \pm j\omega_g$, $s_{7,8} = 0$[rad/s]. The first six poles, $s_{1\div4}$ and $s_{5,6}$, originate from the LCL filter model that are additionally shifted by terms $\pm j\omega_g$ owing to the transformation from the stationary to the rotational dq frame. The pole pair, $s_{7,8}$, originates from two synchronization integrators.

One of the means to provide the required level of damping to the system is to add a MIMO compensator:

$$\underline{u}_{iA} = -\underline{K} \cdot \begin{bmatrix} \underline{i}_{Li} \\ \underline{u}_{Cf} \\ \underline{i}_{Lg} \\ \underline{u}_S \end{bmatrix}, \tag{30}$$

that forms the feedback control loop based on the state variables and effectively shifts the location of the closed-loop system poles deeper into the left half-plane. The obtained control variable, $u_{iA} = \begin{bmatrix} u_{iAd} & u_{iAq} \end{bmatrix}^T$, must be realized as an additional PU output voltage component, as shown in Fig. 7, which provides the active damping effect. The state-feedback gain matrix, $K$, is determined such that the eigenvalues of the closed-loop system matrix $\underline{A}$-$\underline{B}_i \cdot \underline{K}$ correspond to the preferred pole locations. The algorithm given in [41] accepts the vector of the preferred pole locations, $p$, and uses the inherent additional degree of freedom to minimize the sensitivity of the closed-loop system to, either, the disturbances, or the variations in system parameters (in this paper, the form of the algorithm that seeks the solution with minimal sensitivity to the variation in system parameters has been implemented).

### E. EXAMPLE OF THE ACTIVE DAMPING STATE-FEEDBACK MATRIX CALCULATION

The filter model, including synchronization error integrators, with parameters given in the design example from the previous chapter, is characterized by the following set of poles:

$$s_{1,2} = \pm j\left(\omega_{res} + \omega_g\right) = 0 \pm j17157\frac{\text{rad}}{\text{s}},$$
$$s_{3,4} = \pm j\left(\omega_{res} - \omega_g\right) = 0 \pm j16529\frac{\text{rad}}{\text{s}},$$
$$s_{5,6} = \pm j\omega_g = 0 \pm j314\frac{\text{rad}}{\text{s}}, \quad s_{7,8} = 0 \pm j0\frac{\text{rad}}{\text{s}}.$$

Setting the damping time constant for the closed-loop system poles to 2.5 ms, the new poles' location becomes:

$$p_{1,2} = -400 \pm j17157\frac{\text{rad}}{\text{s}}, \quad p_{3,4} = -400 \pm j16529\frac{\text{rad}}{\text{s}},$$
$$p_{5,6} = -400 \pm j314\frac{\text{rad}}{\text{s}}, \quad p_{7,8} = -400 \pm j0\frac{\text{rad}}{\text{s}}$$

After applying the poles' placement algorithm, the obtained state-feedback matrix coefficients are given in Table 2 in the $PU_1$ control parameters setup section. The active damping and synchronization algorithm was tested within a micro-grid simulation model and the results are presented in the Chapter IV.

## IV. SIMULATION RESULTS

The performance of the proposed concept for decentralized P2P-based power flow control, coupling filter design, and active damping and synchronization control has been validated in a Matlab/Simulink model of a simple radial MG in the off-grid mode of operation [15] shown in Fig. 8. The main goal is to confirm the hypothesis that the concept can considerably improve the static and dynamic characteristics of the system in comparison to the conventional decentralized droop method. Also, the level of influence of the communication time-delay between the contractees has been investigated.

The MG model consists of a feeder, three PUs, and three passive loads ($P_L$+$jQ_L$). Using dedicated switches, the PUs and loads can be connected to or disconnected from the feeder. The system parameters are listed in Table 1. It is assumed that a PU can source or sink the active power $P_{PU}$, and/or the reactive power, $Q_{PU}$, up to the given power rating level, where their positive sign corresponds to PU sourcing the power. DC bus of each PU is modeled by the constant voltage source. This represents functionally essential, controlled DC energy storage at PU's DC bus. The loads are modeled as a three-phase star-connected series of a resistance and inductance (the positive sign of the active power, $P_L$, and of the reactive power, $Q_L$, corresponds to the power consumption). It should be noted that each PU coupling filter was designed according to its rated power and procedure given in Chapter III.

In addition to the droop control and active damping, the modeled PU control algorithm comprises the space-vector modulator block, switching at $f_{SW}$, and the PLL block based on the PI controller (with $K_{Ppll}$ and $K_{Ipll}$ gains) that measures the corresponding PCC angular frequency ($\omega$) and PCC voltage magnitude ($U_{m1}$ or $U_{m2}$ or $U_{m3}$). The transfer functions of the integrator elements in Eqs. (4), (5), and (29) (i.e., Fig. 7),

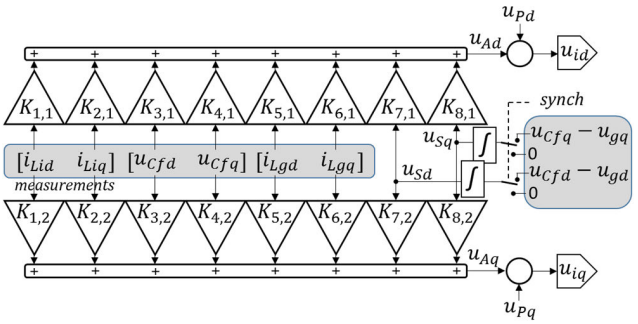


**FIGURE 7.** Active damping and synchronization algorithm.

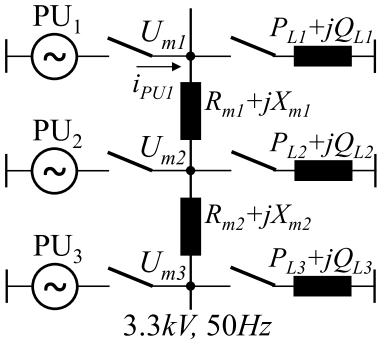


**FIGURE 8.** Setup of the test MG.

and the integral term in the PLL block were discretized using the bilinear transformation. The sampling period of the active damping and the PLL block was set equal to the switching period, $1/f_{SW}$, while the droop control sampling period, $T_P$, is set to be an order of magnitude higher, $T_P = 1$ ms. The control parameters and their values are listed in the Table 2.

The tests conducted on the MG model covered three scenarios regarding the level of communication layer involvement in the system's power flow control: a) without the communication layer – PUs implement the conventional decentralized droop-based power flow control, b) with the decentralized P2P based power flow control between the PUs and passive loads, and c) with the decentralized P2P based power flow control involving solely PUs. The tests have a common outline, as shown in Fig. 9: at 0.15 s $PU_1$ is connected to the MG, at 0.5 s load 2 is connected, and so on. It should be noted that $PU_1$ served as a MG voltage forming unit, while $PU_2$ and $PU_3$ needed to be synchronized prior to the connection.

The first testing scenario verified the performance of the MG where PUs were implementing the conventional decentralized droop control.

Plots of the instantaneous active powers, $p_{PU1}$, $p_{PU2}$, and $p_{PU3}$ and plots of the instantaneous reactive powers, $q_{PU1}$, $q_{PU2}$, and $q_{PU3}$, are shown in Fig. 10. Their quasi-steady-state values attained after each new element is switched-on, are given in Table 3. They confirm that the combined action of the connected PUs bring almost equal relative load power sharing (expressed in $[\%\cdot S_N]$) among the units in quasi-steady states.

However, plots of the angular frequency, $\omega$, and of grid voltages' magnitudes $U_{m1}$, $U_{m2}$, $U_{m3}$ show their prompt responses to the connection or disconnection of any MG component or to any change in their power throughput (please note that the signal $U_{m3}$ is overlapped by signal $U_{m2}$). Their quasi-steady-state shifts are the matter of secondary controllers' corrective action, but the MG frequency and voltage magnitude rate of change might not be acceptable to sensitive loads or utility equipment. Additionally, the response of the voltage $u_{m2}$ and response of the $PU_1$ output current, $i_{PU1}$, as well as plots of the instantaneous active and reactive powers from Fig. 10, prove the effectiveness of the applied coupling filter active damping and synchronization control method: synchronization process of $PU_2$ and $PU_3$ to the MG voltage did not produce any disruption effects to the system variables (there are no spikes in magnitude and transitional oscillations).

The second test incorporated decentralized P2P-based power flow control, where the testing scenario assumed power delivery contracts between pair of a PU and a passive load. Passive loads participated in power flow control by measuring and communicating their instantaneous active and reactive power consumption to a particular PU to level their power output. In the presented case, the contractees were $PU_1$ and $load_2$, $PU_2$ and $load_3$, and $PU_3$ and $load_1$. One of the most critical parameters for the system performance is the communication delay that indirectly introduces a time mismatch in the contractees' power flows, thus provoking disruptions to the system. To gain insight into the level of its influence, system responses for the zero-communication delay and 20 ms communication delay were contrasted in Fig. 11.a and Fig. 11.b, respectively.

Considering that a relatively low data volume is transmitted over short distances, a delay below 20 ms could be deemed attainable [16], [32]. The plots of the angular frequency and grid voltages show superior quasi-steady-state performance in comparison with the conventional droop control: quasi-steady-state magnitudes of $\omega$, $U_{m1}$, $U_{m2}$, and $U_{m3}$ remained almost unchanged at their initial levels throughout the periods of the power contract settlements (please note that the signal $U_{m3}$ is overlapped by signal $U_{m2}$).

The active and reactive power outputs of the PUs correctly tracked the corresponding load demands ($P_{PU1} \approx P_{L2}$, $Q_{PU1} \approx Q_{L2}$, $P_{PU2} \approx P_{L3}$, $Q_{PU2} \approx Q_{L3}$, $P_{PU3} \approx P_{L1}$, $Q_{PU3} \approx Q_{L1}$), being barely disturbed by the line power losses and the voltage drop along the line. This feature may, to a great extent, relieve the control action of the frequency and voltage secondary controllers. In the transitional periods, $\omega$ and MG voltages still suffer perturbation with a high rate of change, although of the considerably lower magnitude compared to the conventional control. This clear confirmation of enhanced dynamical performance provided by the decentralized P2P-based power flow control faces noticeable regression in the presence of communication delay, however, as the high rate of frequency and voltage perturbations

**TABLE 1. Parameters of the MG, PUs and loads.**

| | | |
|---|---|---|
| MG line-to-line voltage | | $U_N$ =3300 *V* |
| MG angular frequency | | $\omega_N$ =314 *rad/s* |
| MG feeder | | $R_{m1}$= $R_{m2}$=100 *mΩ*; $L_{m1}$= $L_{m2}$=1 *mH* |
| $PU_1$ | *power rating* | $P_{PU1}$=0.42 *MW*, $Q_{PU1}$=0.42 *MVAr* |
| | *DC bus voltage* | $U_{DC1}$=6.9 *kV* |
| | *LCL filter* | $L_{i1}$=1.5 *mH*, $Cf_1$=4.7 *μF*, $L_{g1}$=1.5 *mH* |
| $PU_2$ | *power rating* | $P_{PU2}$=0.21 *MW*, $Q_{PU2}$=0.21 *MVAr* |
| | *DC bus voltage* | $U_{DC2}$=6.9 *kV* |
| | *LCL filter* | $L_{i2}$=3.3 *mH*, $Cf_2$=2.3 *μF*, $L_{g2}$=3.3 *mH* |
| $PU_3$ | *power rating* | $P_{PU3}$=0.14 *MW*, $Q_{PU3}$=0.14 *MVAr* |
| | *DC bus voltage* | $U_{DC3}$=6.9 *kV* |
| | *LCL filter* | $L_{i3}$=4.7 *mH*, $Cf_3$=1.6 *μF*, $L_{g3}$=4.7 *mH* |
| $load_1$ | | $P_{L1}$=200 *kW*, $Q_{L1}$=100 *kVAr* (series) |
| $load_2$ | | $P_{L2}$=200 *kW*, $Q_{L2}$=100 *kVAr* (series) |
| $load_3$ | | $P_{L3}$=200 *kW*, $Q_{L3}$=100 *kVAr* (series) |

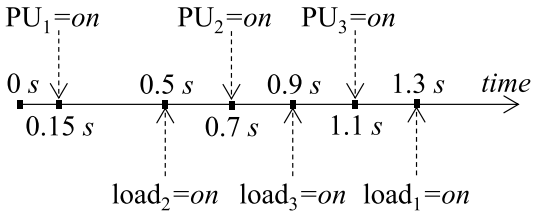


**FIGURE 9. Test outline.**

increased. The obtained instantaneous power responses of $p_{PU}$ and $q_{PU}$ show another potential limitation in the concept applicability. Namely, the presence of a passive or uncontrollable load of relatively high power in the very vicinity of a particular PU would frequently disturb the unit and provoke it to invest considerable power capacities into the frequency and the PCC voltage regulation, leaving it with less room for trading. The solution to the problem might be a power flow control method that would impose limited PU's power output for supporting the MG stability. The results have shown another interesting conclusion: as the number of connected PUs increases (two PUs after 0.9 s and three PUs after 1.3 s), the MG becomes stiffer, and perturbations are more dumped.

The same simulation model and testing scenario was used to verify the proposed LCL filter design methodology. *THDU* was measured at the MG's 2nd node ($THDU_{m2}$) at each quasi-steady-state and $HDI_{(200)}$ ($h = 200$ corresponds to the switching frequency sideband) was measured at the $PU_1$ micro-grid connection point. The obtained values are noted alongside the voltage magnitude plots in Fig. 11.a.

The highest *THDU* value was recorded in the MG's no-load state ($t < 0.5$ s), thus confirming the conclusion of the high-frequency PUs-to-passive loads interaction study. The connection of a new load only slightly decreases the *THDU* value (by 0.05%) because of the relatively high impedance of the load. As expected, the connection of the new PU leads to a slight increase (by 0.05%) in the THDU which is determined by the feeder impedance. In total, the recorded maximal value of 1.3% is well below the IEEE 519-2014 standard *THDU* limit of 5%.

**TABLE 2. Control parameters.**

| | | |
|---|---|---|
| $PU_1$ | droop | $K_{\omega 1}$=14.95·10$^{-6}$, $K_{u1}$=1.6·10$^{-3}$, $K_{Pu1}$=50·10$^{-3}$, $K_{Iu1}$=10·$K_{Pu1}$ |
| | active damping | $K_{1,1}$=2.38, $K_{1,2}$=78.5*m*, $K_{1,3}$= -4.80*m*, $K_{1,4}$= -13.5*m*, $K_{1,5}$= -1.11, $K_{1,6}$= -1.46, $K_{1,7}$=719, $K_{1,8}$=974, $K_{2,1}$=33.8*m*, $K_{2,2}$=2.42, $K_{2,3}$= -12*m*, $K_{2,4}$=18.4*m*, $K_{2,5}$=1.66, $K_{2,6}$= -1.31, $K_{2,7}$= -1062, $K_{2,8}$=89.6 |
| | PLL, $f_{SW}$, $T_P$ | $K_{Ppll}$=6.1*m*, $K_{Ipll}$=30.3*m*, $f_{SW}$=10 *kHz*, $T_P$=1*ms* |
| $PU_2$ | droop | $K_{\omega 2}$=29.90·10$^{-6}$, $K_{u2}$=3.2·10$^{-3}$, $K_{Pu2}$=25·10$^{-3}$, $K_{Iu2}$=10·$K_{Pu2}$ |
| | active damping | $K_{1,1}$=5.37, $K_{1,2}$=69*m*, $K_{1,3}$= -20.3*m*, $K_{1,4}$= -11*m*, $K_{1,5}$= -2.81, $K_{1,6}$= -3.8, $K_{1,7}$=895, $K_{1,8}$=1097, $K_{2,1}$= -0.14, $K_{2,2}$=5.19, $K_{2,3}$= -9.3*m*, $K_{2,4}$= -5.6*m*, $K_{2,5}$=3.0, $K_{2,6}$= -2.51, $K_{2,7}$= -941, $K_{2,8}$=721 |
| | PLL, $f_{SW}$, $T_P$ | $K_{Ppll}$=6.1*m*, $K_{Ipll}$=30.3*m*, $f_{SW}$=10 *kHz*, $T_P$=1*ms* |
| $PU_3$ | droop | $K_{\omega 3}$=44.85·10$^{-6}$, $K_{u3}$=4.8·10$^{-3}$, $K_{Pu3}$=17·10$^{-3}$, $K_{Iu3}$=10·$K_{Pu3}$ |
| | active damping | $K_{1,1}$=2.38, $K_{1,2}$=78.5*m*, $K_{1,3}$= -4.80*m*, $K_{1,4}$= -13.5*m*, $K_{1,5}$= -1.11, $K_{1,6}$= -1.46, $K_{1,7}$=719, $K_{1,8}$=974, $K_{2,1}$=33.8*m*, $K_{2,2}$=2.42, $K_{2,3}$= -12*m*, $K_{2,4}$=18.4*m*, $K_{2,5}$=1.66, $K_{2,6}$= -1.31, $K_{2,7}$= -1062, $K_{2,8}$=89.6 |
| | PLL, $f_{SW}$, $T_P$ | $K_{Ppll}$=6.1*m*, $K_{Ipll}$=30.3*m*, $f_{SW}$=10 *kHz*, $T_P$=1 *ms* |

**TABLE 3. Quasi steady state power levels throughout the first test scenario.**

| $t >$ | 0.5 s | 0.7 s | 0.9 s | 1.1 s | 1.3 s |
|---|---|---|---|---|---|
| $P_{PU1}$ [$W$·10$^5$] | 1.8 | 1.23 | 2.33 | 1.93 | 2.81 |
| $Q_{PU1}$ [$W$·10$^5$] | 0.99 | 0.65 | 1.24 | 1.02 | 1.49 |
| $P_{PU2}$ [$W$·10$^5$] | | 0.61 | 1.16 | 0.97 | 1.41 |
| $Q_{PU2}$ [$W$·10$^5$] | | 0.35 | 0.67 | 0.54 | 0.77 |
| $P_{PU3}$ [$W$·10$^5$] | | | | 0.65 | 0.94 |
| $Q_{PU3}$ [$W$·10$^5$] | | | | 0.37 | 0.52 |
| $P_{PU1}$ [%·$S_N$] | 42.9 | 29.3 | 55.5 | 46.0 | 67.0 |
| $P_{PU2}$ [%·$S_N$] | | 29.1 | 55.2 | 46.2 | 67.1 |
| $P_{PU3}$ [%·$S_N$] | | | | 46.4 | 67.1 |
| $Q_{PU1}$ [%·$S_N$] | 23.6 | 15.5 | 29.5 | 24.3 | 35.5 |
| $Q_{PU2}$ [%·$S_N$] | | 16.7 | 31.9 | 25.7 | 37.7 |
| $Q_{PU3}$ [%·$S_N$] | | | | 26.4 | 37.1 |

The readings of $HDI_{(200)}$ show considerably higher current harmonic attenuation in the micro-grid's off-grid mode than in its on-grid mode (0,022% comparing to 0,055%) and values much below the standard's limits of 0,3% (note also that in this test $PU_1$ is loaded by ∼1/3 of the nominal current). This verifies the *THDU* vs *THDI* correlation study of the micro-grid system given in the previous section.

The third test examines the decentralized P2P-based power flow control performance within the MG hosting solely PUs. Here, the same test outline from Fig. 9 was used to appoint

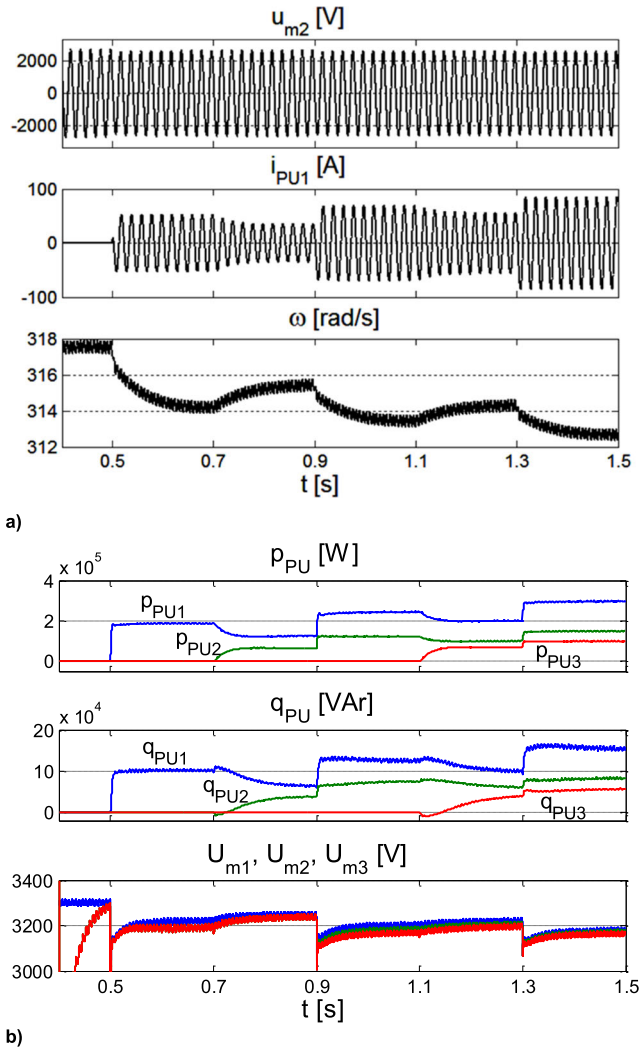


**FIGURE 10.** MG response having PUs implementing conventional decentralized droop control.

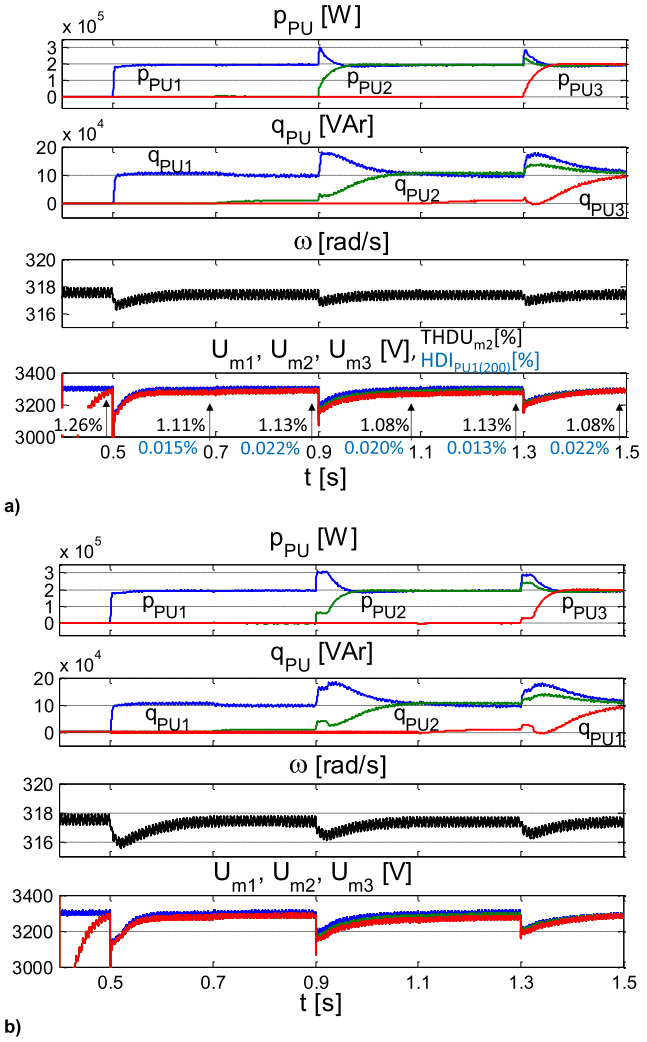


**FIGURE 11.** Decentralized P2P based power flow control tested in the scenario where the passive loads are communicating instantaneous power consumption with: a) zero communication delay; b) 20 ms communication delay.

the following PUs' connection instants and the corresponding power contracts (passive loads are disconnected):

- 0.8 s: the $PU_1$ is to supply 0.12 MW to the $PU_2$;
- 1,2 s: the $PU_1$ active power delivery to the $PU_2$ is halved to 0,06 MW and the $PU_3$ is to supply 0.12 MW to $PU_2$.

Under the assumption that the unit issuing the power transfer can schedule its power intake or its power output at least the delay time in advance of the real execution (utilizing battery storage or smart-home, IoT, or other electrical power management systems), the responding PU would receive the trading instructions before the real execution.

In this way, the communication delay would be bypassed, and the responding unit would be able to settle the power contract in the real time. With such provisions, the obtained responses of instantaneous active power flows, $p_{PU1}$, $p_{PU2}$, and $p_{PU3}$, shown in Fig. 12, show almost perfect power settlement not only in the quasi-steady state, but also during the transitional periods. These reflect in angular frequency and MG voltages responses without perturbations (please note that the signal $U_{m3}$ is overlapped by signal $U_{m2}$).

*THDU* Measurements of the voltage $U_{m2}$ showed maximal reading when $PU_1$ alone was connected to the MG ($t < 0.8$ s) and, thereby working in the idle mode (equivalent to the off-grid mode of operation). This is in agreement with the *THDU* study of the active PCC case.

From the results obtained and observations made on three MG control scenarios, it can be confirmed that the application of the proposed decentralized P2P-based power flow control can considerably enhance both the steady-state and dynamic characteristics of an MG system. Measurements of the power quality in quasi-steady states confirm that *THDU* requirements should be used as a PUs coupling filter design criteria and its disconnected state taken as a critical operating condition.

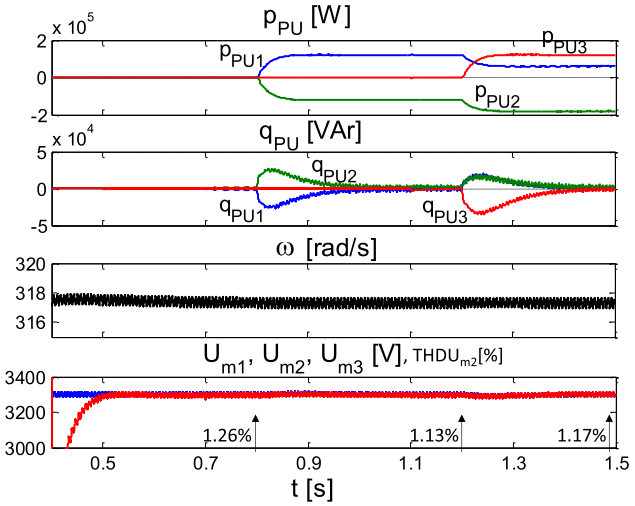


**FIGURE 12.** Decentralized P2P based power flow control tested within the MG hosting solely PUs.

## V. CONCLUSION

This paper proposes a new decentralized control strategy for prosumer units which integrates the energy-exchanging (trading) layer, communication layer, and primary energy flow control layer to execute the so-called ''decentralized peer-to-peer based power flow control algorithm''. It aims at attaining two control objectives simultaneously: 1) the close-to-real-time power flow settlement between involved microgrid units and 2) control of the microgrid frequency and voltage. Structurally, proposed algorithm is an extension of the conventional microgrid voltage and frequency-droop control method in a way that it employs feed-forward control terms of contracted and communicated instantaneous active and reactive power references. These terms actually convert the perturbations in the generated and consumed power flows into control variables. They also provide for operation with positive and negative contracted power values and smooth transition from one to the another, which is a compulsory feature of a prosumer unit.

Having in mind a huge importance of the voltage quality generated by prosumer units as grid-forming units in a microgrid, the paper has addressed the problem of their coupling filter design, active damping of the filter's inherent resonance and prosumer unit's synchronization control to meet the specifications and requirements of the microgrid system. Common iterative LCL coupling filter design procedure has been complemented with the requirement to attain the limited total voltage harmonic distortion as the critical design criterion in the microgrid off-grid mode of operation. In order to understand a PU's influence on the microgrid performance and influence of the microgrid on a PU's performance regarding high-order harmonic distortion, a study was conducted that considered different edge-cases of MG setup as perceived from the PU side of the PCC. The study revealed that the disconnected state of PU is the critical operating condition for meeting the *THDU* requirements inside one microgrid system and for its coupling filter design. The control of the filter dynamics, including active damping and flawless synchronization to the point-of-common coupling voltage, has been resolved by employing a multiple-input-multiple-output controller in the form of a state-feedback gain matrix. Each step of the presented LCL filter design process was backed up by an example.

The proposed decentralized peer-to-peer-based power flow control methodology was verified employing a simple radial microgrid model in the off-grid (islanded) mode of operation. Comparative tests of the conventional and proposed control methodology have confirmed that communicated and feed-forwarded power references can considerably enhance both the steady-state and dynamic characteristics of the MG system. Namely, real-time power contracts settlement ensures almost unchanged quasi-steady-state value of MG frequency and magnitude of MG nods' voltages as PUs and loads are being connected or disconnected. Also, on a relatively smaller time scale it noticeably reduces transitional perturbations in the system variables. This valuable influence on the MG performance grows with the increasing number of PUs installed in a MG. On the other hand, presence of passive and uncontrollable loads and the communication delay has shown a degrading impact on the system dynamics and offers a ground for further control algorithm development.

There are other major aspects of the topic to be considered in the future research, such as: stability analysis of the proposed control concept applied in a microgrid of different topology and a range of system parameters; analysis of influence of spatial distribution and number of installed prosumer units on quasi-steady state voltage excursions at the grid nods; application of advanced decentralized control techniques to enhance dynamical, steady state and fault ride through properties of the peer-to-peer energy exchange concept; inter-microgrid and large scale implementation analysis (dynamical, steady state and fault ride through); providing a frame for the P2P trading platform that meets restrictions coming from the previously noted issues. The overall system performance can be further improved by employing advanced primary level control techniques such as accurate reactive power sharing approach [42], non-linear load current sharing [21], [25], [43] and damping frequency fluctuations [44], [45]. These and other methods, coupled with the proposed P2P energy exchange, can expand the prospects of PUs' utilization in a MG environment. On the other hand, there are many theoretical and practical features of the communication medium and communication protocol to be resolved that correlates with the stability (such as providing maximal guarantied latency), reliability (e.g. resistance to cyber attacks) and scalability, which makes the topic multidisciplinary. Also, all of these require different theoretical, modeling and verification approaches be applied.

## REFERENCES

[1] D. P. Simatupang and J. Choi, "Integrated photovoltaic inverters based on unified power quality conditioner with voltage compensation for submarine distribution system," *Energies*, vol. 11, no. 11, p. 2927, Oct. 2018.

[2] (Apr. 2018). *Monitor Deloitte: Power Market Study 2030: A New Outlook for the Energy Industry*. [Online]. Available: https://www2.deloitte.com/content/dam/Deloitte/de/Documents/energy-resources/Deloitte-Power-Market-Study-2030-EN.pdf

[3] A. M. Eltamaly, M. A. Alotaibi, A. I. Alolah, and M. A. Ahmed, "A novel demand response strategy for sizing of hybrid energy system with smart grid concepts," *IEEE Access*, vol. 9, pp. 20277–20294, 2021, doi: 10.1109/ACCESS.2021.3052128.

[4] *The Coalition for Energy Savings: EU Energy Efficiency Directive (2012/27/EU)*, 2nd ed. Guidebook for Strong Implementation, Brussels, Belgium, 2013.

[5] K. Zhang, S. Troitzsch, S. Hanif, and T. Hamacher, "Coordinated market design for peer-to-peer energy trade and ancillary services in distribution grids," *IEEE Trans. Smart Grid*, vol. 11, no. 4, pp. 2929–2941, Jul. 2020.

[6] E. Mengelkamp, J. Gärttner, K. Rock, S. Kessler, L. Orsini, and C. Weinhardt, "Designing microgrid energy markets: A case study: The Brooklyn Microgrid," *Appl. Energy*, vol. 210, pp. 870–880, Jan. 2018.

[7] W. Du, Q. Jiang, M. J. Erickson, and R. H. Lasseter, "Voltage-source control of PV inverter in a CERTS microgrid," *IEEE Trans. Power Del.*, vol. 29, no. 4, pp. 1726–1734, Aug. 2014.

[8] J. Rocabert, A. Luna, F. Blaabjerg, and P. Rodríguez, "Control of power converters in AC microgrids," *IEEE Trans. Power Electron.*, vol. 27, no. 11, pp. 4734–4749, Nov. 2012.

[9] M. Yan, M. Shahidehpour, A. Paaso, L. Zhang, A. Alabdulwahab, and A. Abusorrah, "Distribution network-constrained optimization of peer-to-peer transactive energy trading among multi-microgrids," *IEEE Trans. Smart Grid*, vol. 12, no. 2, pp. 1033–1047, Mar. 2021.

[10] B. V. Rao, M. Stefan, R. Schwalbe, F. Zeilinger, A. Schenk, A. Frischenschlager, P. Stetn, and G. Taljan, "Grid capacity management for peer-to-peer local energy communities," in *Proc. IEEE Power Energy Soc. Gen. Meeting (PESGM)*, Montreal, QC, Canada, Aug. 2020, pp. 1–5.

[11] S. Wang, A. F. Taha, J. Wang, K. Kvaternik, and A. Hahn, "Energy crowdsourcing and peer-to-peer energy trading in blockchain-enabled smart grids," *IEEE Trans. Syst., Man, Cybern., Syst.*, vol. 49, no. 8, pp. 1612–1623, Aug. 2019.

[12] C. Roncero-Clemente, E. Gonzalez-Romera, F. Barrero-González, M. I. Milanés-Montero, and E. Romero-Cadaval, "Power-flow-based secondary control for autonomous droop-controlled AC nanogrids with peer-to-peer energy trading," *IEEE Access*, vol. 9, pp. 22339–22350, 2021.

[13] Y. Yang and R.-J. Wai, "Design of adaptive fuzzy-neural-network-imitating sliding-mode control for parallel-inverter system in islanded micro-grid," *IEEE Access*, vol. 9, pp. 56376–56396, 2021.

[14] W. Kohn, Z. B. Zabinsky, and A. Nerode, "A micro-grid distributed intelligent control and management system," *IEEE Trans. Smart Grid*, vol. 6, no. 6, pp. 2964–2974, Nov. 2015.

[15] M. C. Chandorkar, D. M. Divan, and R. Adapa, "Control of parallel connected inverters in standalone AC supply systems," *IEEE Trans. Ind. Appl.*, vol. 29, no. 1, pp. 136–143, Jan. 1993.

[16] S. F. Bush, S. Goel, and G. Simard, *Smart Grid Research: Communications—IEEE Vision for Smart Grid Communications: 2030 and Beyond Roadmap*, IEEE Communications Society, New York, NY, USA, Dec. 2013.

[17] S. Marzal, R. Salas-Puente, R. Gonzalez-Medina, E. Figueres, and G. Garcera, "Peer-to-peer decentralized control structure for real time monitoring and control of microgrids," in *Proc. IEEE 26th Int. Symp. Ind. Electron. (ISIE)*, Edinburgh, U.K., Jun. 2017, pp. 140–145.

[18] Y. Khayat, Q. Shafiee, R. Heydari, M. Naderi, T. Dragicevic, J. W. Simpson-Porco, F. Dörfler, M. Fathi, F. Blaabjerg, J. M. Guerrero, and H. Bevrani, "On the secondary control architectures of AC microgrids: An overview," *IEEE Trans. Power Electron.*, vol. 35, no. 6, pp. 6482–6500, Jun. 2020.

[19] N. W. A. Lidula and A. D. Rajapakse, "Voltage balancing and synchronization of microgrids with highly unbalanced loads," *Renew. Sustain. Energy Rev.*, vol. 31, pp. 907–920, Mar. 2014.

[20] X. Wang, J. Qi, Y. Hou, Y. Wang, W. Xu, D. Wang, and Z. Jiao, "Studies on fault analysis and protection configuration schemes in an isolated microgrid," in *Proc. IEEE PES Gen. Meeting Conf. Expo.*, National Harbor, MD, USA, Jul. 2014, pp. 1–5.

[21] N. Khosravi, H. R. Abdolmohammadi, S. Bagheri, and M. R. Miveh, "A novel control approach for harmonic compensation using switched power filter compensators in micro-grids," *IET Renew. Power Gener.*, vol. 15, no. 16, pp. 3989–4005, Oct. 2021.

[22] N. Khosravi, S. Echalih, R. Baghbanzadeh, Z. Hekss, R. Hassani, and M. Messaoudi, "Enhancement of power quality issues for a hybrid AC/DC microgrid based on optimization methods," *IET Renew. Power Gener.*, vol. 16, no. 8, pp. 1773–1791, Apr. 2022.

[23] N. Khosravi, H. R. Abdolmohammadi, S. Bagheri, and M. R. Miveh, "Improvement of harmonic conditions in the AC/DC microgrids with the presence of filter compensation modules," *Renew. Sustain. Energy Rev.*, vol. 143, Jun. 2021, Art. no. 110898.

[24] N. Khosravi, S. Echalih, Z. Hekss, R. Baghbanzadeh, M. Messaoudi, and M. Shahideipour, "A new approach to enhance the operation of M-UPQC proportional-integral multiresonant controller based on the optimization methods for a stand-alone AC microgrid," *IEEE Trans. Power Electron.*, vol. 38, no. 3, pp. 3765–3774, Mar. 2023.

[25] F. Göthner, J. Roldán-Pérez, R. E. Torres-Olguin, and O. -M. Midtgård, "Harmonic virtual impedance design for optimal management of power quality in microgrids," *IEEE Trans. Power Electron.*, vol. 36, no. 9, pp. 10114–10126, Sep. 2021.

[26] J. C. Lai, H. S. Chung, Y. He, W. Wu, and F. Blaabjerg, "Wideband series harmonic voltage compensator for enhancing stability of microgrids," *IEEE Trans. Power Electron.*, vol. 37, no. 8, pp. 9687–9702, Aug. 2022.

[27] K. Jalili and S. Bernet, "Design of *LCL* filters of active-front-end two-level voltage-source converters," *IEEE Trans. Ind. Electron.*, vol. 56, no. 5, pp. 1674–1689, May 2009.

[28] R. Peña-Alzola, M. Liserre, F. Blaabjerg, M. Ordonez, and Y. Yang, "*LCL*-filter design for robust active damping in grid-connected converters," *IEEE Trans. Ind. Informat*, vol. 10, no. 4, pp. 2192–2203, Nov. 2014.

[29] F. Huerta, D. Pizarro, S. Cobreces, F. J. Rodriguez, C. Giron, and A. Rodriguez, "LQG servo controller for the current control of *LCL* grid-connected voltage-source converters," *IEEE Trans. Ind. Electron.*, vol. 59, no. 11, pp. 4272–4284, Nov. 2012.

[30] E. Barklund, N. Pogaku, M. Prodanovic, C. Hernandez-Aramburo, and T. C. Green, "Energy management in autonomous microgrid using stability-constrained droop control of inverters," *IEEE Trans. Power Electron.*, vol. 23, no. 5, pp. 2346–2352, Sep. 2008.

[31] I. Isakov, M. Vekić, M. Rapaić, I. Todorović, and S. Grabić, "Decentralized self-stabilizing primary control of microgrids," *Int. J. Electr. Power Energy Syst.*, vol. 155, Jan. 2024, Art. no. 109477, doi: 10.1016/j.ijepes.2023.109477.

[32] (May 6, 2023). *3GPP—The 5G Standard—Highlights*. [Online]. Available: https://www.3gpp.org/newsletter-issue-06-may-2023

[33] A. A. Alkahtani, S. T. Y. Alfalahi, A. A. Athamneh, A. Q. Al-Shetwi, M. B. Mansor, M. A. Hannan, and V. G. Agelidis, "Power quality in microgrids including supraharmonics: Issues, standards, and mitigations," *IEEE Access*, vol. 8, pp. 127104–127122, 2020.

[34] M. H. J. Bollen, J. Zhong, F. Zavoda, J. Meyer, A. McEachern, and F. C. Lopez, "Power quality aspects of smart grids," in *Proc. Intern. Conf. Renewable Energy Power Quality (ICREPQ)*, vol. 1, no. 8, Granada, Spain, Mar. 2010, pp. 1061–1066.

[35] Y. Du, D. D. Lu, D. Cornforth, and G. James, "A study on the harmonic issues at CSIRO microgrid," in *Proc. IEEE 9th Int. Conf. Power Electron. Drive Syst.*, Singapore, Dec. 2011, pp. 203–207.

[36] Z. Zeng, H. Yang, C. Cheng, Z. Zeng, and R. Zhao, "Harmonic and reactive currents sharing by multi-functional grid-connected inverters in a microgrids," in *Proc. 15th Int. Conf. Elect. Mach. Syst. (ICEMS)*, Sapporo, Japan, Oct. 2012, pp. 1–5.

[37] M. Liserre, A. Dell'Aquila, and F. Blaabjerg, "Genetic algorithm-based design of the active damping of an *LCL*-filer three-phase active rectifier," *IEEE Trans. Power Electron.*, vol. 19, no. 1, pp. 76–86, Jan. 2004.

[38] C. Wessels, J. Dannehl, and F. W. Fuchs, "Active damping of LCL-filter resonance based on virtual resistor for PWM rectifiers—Stability analysis with different filter parameters," in *Proc. IEEE Power Electron. Specialists Conf.*, Rhodes, Greece, Jun. 2008, pp. 3532–3538.

[39] B. Bahrani, M. Vasiladiotis, and A. Rufer, "High-order vector control of grid-connected voltage-source converters with LCL-filters," *IEEE Trans. Ind. Electron.*, vol. 61, no. 6, pp. 2767–2775, Jun. 2014.

[40] E. Wu and P. W. Lehn, "Digital current control of a voltage source converter with active damping of LCL resonance," *IEEE Trans. Power Electron.*, vol. 21, no. 5, pp. 1364–1373, Sep. 2006.

[41] J. Kautsky, N. K. Nichols, and P. Van Dooren, "Robust pole assignment in linear state feedback," *Int. J. Control*, vol. 41, no. 5, pp. 1129–1155, Jul. 1985.

[42] Y. W. Li and C.-N. Kao, "An accurate power control strategy for power-electronics-interfaced distributed generation units operating in a low-voltage multibus microgrid," *IEEE Trans. Power Electron.*, vol. 24, no. 12, pp. 2977–2988, Dec. 2009.
[43] J. He, Y. W. Li, J. M. Guerrero, F. Blaabjerg, and J. C. Vasquez, "An islanding microgrid power sharing approach using enhanced virtual impedance control scheme," *IEEE Trans. Power Electron.*, vol. 28, no. 11, pp. 5272–5282, Nov. 2013.
[44] M. Eskandari, L. Li, M. H. Moradi, P. Siano, and F. Blaabjerg, "Active power sharing and frequency restoration in an autonomous networked microgrid," *IEEE Trans. Power Syst.*, vol. 34, no. 6, pp. 4706–4717, Nov. 2019.
[45] Y. Geng, L. Zhu, X. Song, K. Wang, and X. Li, "A modified droop control for grid-connected inverters with improved stability in the fluctuation of grid frequency and voltage magnitude," *IEEE Access*, vol. 7, pp. 75658–75669, 2019.

**STEVAN GRABIĆ** (Member, IEEE) received the B.S., M.S., and Ph.D. degrees in electrical engineering and computer sciences from the Faculty of Technical Sciences, University of Novi Sad, Serbia. After receiving the Ph.D. degree, in 2011, he has been with the Department of Power Electronics and Electrical Machines, University of Novi Sad. Since 2017, he has been an Associate Professor teaching power electronics and control of energy converters courses. His current research interests include smart and microgrids, renewable energy sources, and power electronic converters.

**MARKO VEKIĆ** (Member, IEEE) received the B.S., M.S., and Ph.D. degrees from the Faculty of Technical Sciences, University of Novi Sad, Serbia, in the field of electrical power engineering and power electronics, in 2005, 2007, and 2014, respectively. Since 2005, he has been with the Department of Power Electronics and Electrical Machines, University of Novi Sad. Since 2019, he has been an Associate Professor teaching the application of power electronics in transmission and distribution grids and electrical power quality courses. His current research interests include smart grids, grid-connected power electronic converters, and renewable energy sources.

**MILAN RAPAIĆ** (Member, IEEE) received the B.S., M.S., and Ph.D. degrees in the field of control theory from the Faculty of Technical Sciences, University of Novi Sad, Serbia, in 2005, 2007, and 2011, respectively. Since 2007, he has held several researchers and teaching positions, and since 2021, he has been a Full Professor with the Computing and Control Department, University of Novi Sad. He is teaching control theory, real-time control algorithms, nonlinear and evolution algorithms, and adaptive and advanced control courses. His current research interests include complex dynamics and multi-agent systems, non-convex, evolutionary and swarm-based optimization techniques, intelligent and adaptive systems, and microgrids.

**IVANA ISAKOV** (Member, IEEE) received the B.S. and M.S. degrees in electrical engineering and computer sciences from the Faculty of Technical Sciences, University of Novi Sad, Serbia, in 2016 and 2017, respectively, where she is currently pursuing the Ph.D. degree in electrical engineering and computer sciences. Since 2017, she has been with the Department of Power Electronics and Electrical Machines, University of Novi Sad, where she has been a Teaching Assistant, since 2018. Her current research interests include smart and micro grids, renewable energy sources, and the control of power electronic converters.

**VLADO POROBIĆ** (Member, IEEE) received the B.S., M.S., and Ph.D. degrees in electrical engineering from the Faculty of Technical Sciences, University of Novi Sad, Serbia, in 2000, 2005, and 2012, respectively. Since 2000, he has been with the Department of Power Electronics and Electrical Machines, University of Novi Sad. Since 2017, he has been an Associate Professor with the University of Novi Sad, and since 2019, he has been with Continental Automotive, Novi Sad, as a Senior Software Engineer. His current research interests include the digital control of electric motors, renewable energy sources, the control of industrial processes, and microcontroller-based communications.